Plant Cell Advance Publication. Published on June 11, 2020, doi:10.1105/tpc.20.00015

RESEARCH ARTICLE

Unregulated Sphingolipid Biosynthesis in Gene-Edited Arabidopsis *ORM* Mutants Results in Nonviable Seeds with Strongly Reduced Oil Content

Ariadna Gonzalez-Solis[1†], Gongshe Han[2†], Lu Gan[1†], Yunfeng Liu[1†], Jonathan E. Markham[1], Rebecca E. Cahoon[1], Teresa M. Dunn*[2], and Edgar B. Cahoon*[1]

[1]Center for Plant Science Innovation & Department of Biochemistry, University of Nebraska-Lincoln, Lincoln, NE 68588 USA

[2] Department of Biochemistry, Uniformed Services University of the Health Sciences, Bethesda, MD, 20814 USA

[†]These authors contributed equally to this work

*Corresponding Authors: ecahoon2@unl.edu and teresa.dunn-giroux@usuhs.edu

Short title: ORM-Mediated Sphingolipid Biosynthesis

One-sentence summary: Removing the regulation of sphingolipid biosynthesis by completely knocking out Orosomucoid-like protein (ORM) genes results in ceramide hyperaccumulation and nonviable seeds with strongly reduced oil content.

The authors responsible for distribution of materials integral to the findings presented in this article in accordance with the policy described in the Instructions for Authors (www.plantcell.org) are: Edgar B. Cahoon (ecahoon2@unl.edu) and Teresa M. Dunn (teresa.dunn-giroux@usuhs.edu).

ABSTRACT

Orosomucoid-like proteins (ORMs) interact with serine palmitoyltransferase (SPT) to negatively regulate sphingolipid biosynthesis, a reversible process critical for balancing the intracellular sphingolipid levels needed for growth and programmed cell death. Here we show that ORM1 and ORM2 are essential for lifecycle completion in *Arabidopsis thaliana.* Seeds from *orm1*$^{-/-}$ *orm2*$^{-/-}$ mutants (generated by crossing CRISPR/Cas9 knockout mutants for each gene) accumulated high levels of ceramide, pointing to

unregulated sphingolipid biosynthesis. *orm1*$^{-/-}$ *orm2*$^{-/-}$ seeds were nonviable, displayed aberrant embryo development, and had >80% reduced oil content vs. wild-type seeds. This phenotype was mimicked in Arabidopsis seeds expressing the SPT subunit LCB1 lacking its first transmembrane domain, which is critical for ORM-mediated regulation of SPT. We identified a mutant for ORM1 lacking one amino acid (Met51) near its second transmembrane domain that retained its membrane topology. Expressing this allele in the *orm2* background yielded plants that did not advance beyond the seedling stage, hyperaccumulated ceramides, and showed altered organellar structures and increased senescence and pathogenesis-related gene expression. These seedlings also showed upregulated expression of genes for sphingolipid catabolic enzymes, pointing to additional mechanisms for maintaining sphingolipid homeostasis. ORM1 lacking Met51 had strongly impaired interactions with LCB1 in yeast (*Saccharomyces cerevisiae*) model), providing structural clues about regulatory interactions between ORM and SPT.

INTRODUCTION

Sphingolipids are essential, abundant endomembrane and plasma membrane lipids that contribute to membrane function, vesicular trafficking, and the mediation of cellular processes in eukaryotes (Coursol *et al.*, 2003; Liang *et al.*, 2003; Chen *et al.*, 2006; Markham *et al.*, 2011). The unique and defining structural feature of sphingolipids is the long-chain base (LCB) or sphingoid base. The simplest LCB, sphinganine (d18:0), derives from the condensation of serine and palmitoyl-CoA catalyzed by serine palmitoyltransferase (SPT) and subsequent reduction of the 3-ketosphinganine product. LCBs can be further modified by hydroxylation, desaturation, and phosphorylation to yield a range of structural variants (Markham *et al.*, 2006; Chen, *et al*., 2009). Free LCBs and their phosphorylated forms typically occur in low concentrations in eukaryotic cells. LCBs exert signaling functions such as modulating cell proliferation and apoptosis in mammalian cells and serve as a trigger of programmed cell death (PCD) and associated pathogen defense responses in plant cells (Alden *et al.*, 2011; Zheng *et al.*, 2018; Huby *et al.*, 2019). The majority of LCBs occur in ceramides. These N-acylated LCBs are synthesized by ceramide synthase-mediated condensation of an LCB and a fatty acyl-CoA. Ceramide synthases have defined substrate specificities that result in ceramides with distinct pairings of structurally diverse LCBs and fatty acids (Markham *et al.*, 2011; Ternes *et al.*, 2011; Luttgeharm, et al., 2015a, Chen, *et al.*, 2015). In mammalian cells, ceramides function as regulators of apoptotic processes;

perturbations in their levels are associated with inflammation, obesity, diabetes and cancer. In plants, ceramide accumulation has been shown to initiate PCD (Liang *et al.*, 2003; Bi *et al.*, 2014; Dadsena *et al.*, 2019). Ceramides provide the hydrophobic backbone for more complex sphingolipids, including glucosylceramides (GlcCer) and glycosylinositolphosphoceramides (GIPCs), the principal glycosphingolipids of plant cells.

SPT activity is highly regulated in eukaryotes to modulate the requirement of sphingolipids for growth and membrane function while limiting the accumulation of LCBs and ceramides until needed to trigger specific cellular functions, such as PCD-mediated pathogen defense in plants (Peer *et al.*, 2010). SPT is composed of the subunits LCB1 and LCB2 and the accessory protein known as small subunit of SPT (ssSPT) or TSC3 in yeast (*Saccharomyces cerevisiae*) (Gable *et al.*, 2000; Kimberlin *et al.*, 2013). SPT is primarily regulated by post-translational mechanisms in order to rapidly respond to perturbations in intracellular sphingolipid concentrations. ORMs or orosomucoid-like proteins (or ORMDL in mammals) are now recognized as non-catalytic proteins that negatively regulate SPT (Breslow *et al.*, 2010; Han *et al.*, 2010). In Arabidopsis (*Arabidopsis thaliana*), two *ORM* genes, *ORM1* (At1g01230) and *ORM2* (At5g42000), were previously identified (Kimberlin *et al.,* 2016). In *Saccharomyces cerevisiae,* Orm1p and Orm2p suppress SPT activity in response to elevated sphingolipid levels through a physical interaction that requires the first transmembrane domain of LCB1 (Han *et al.*, 2019). Sphingolipid-responsive regulation of the ORM-SPT interaction in *S. cerevisiae* is mediated by phosphorylation/dephosphorylation of an N-terminal domain of the ORMs (Breslow *et al.*, 2010). This domain is absent from ORM/ORMDL of multicellular eukaryotes, suggesting that an alternative mechanism regulates the ORM-SPT interaction, such as a recently demonstrated mechanism of direct binding of a ceramide molecule to mammalian ORMDL and yeast ORM to confer negative SPT regulation (Davis *et al.*, 2019). In addition, ORMDL expression levels vary with sphingolipid availability in mammalian cells (Gupta *et al.*, 2015).

S. cerevisiae cells are viable after knockout of the two ORM genes, but they accumulate increased amounts of LCBs and ceramides and are sensitive to tunicamycin, an inducer of ER stress (Breslow *et al.*, 2010). However, a full

understanding of the biochemical and physiological functions of ORM or ORMDL proteins in multi-cellular eukaryotes is only beginning to emerge. A recent report showed that ORMDL proteins are critical for nerve myelination and for suppressing the accumulation of toxic sphingolipid biosynthetic intermediates in mice (Clarke *et al.,* 2019). Downregulation of *ORM2* using an artificial miRNA in an Arabidopsis *ORM1* T-DNA mutant yielded fertile plants with increased accumulation of LCBs and ceramides and early senescence (Li *et al.*, 2016). In addition, RNAi-induced suppression of Arabidopsis *ORM1* and *ORM2* resulted in plants with a normal appearance but with increased sensitivity to the ceramide synthase inhibitor fumonisin B1 and increased LOH2 ceramide synthase activity (Kimberlin *et al.*, 2016). Beyond Arabidopsis, RNAi of *ORM* genes in rice (*Oryza sativa*) was linked to reduced pollen viability (Chueasiri *et al.*, 2014). However, the lack of complete ORM knockout mutants in Arabidopsis or other plants has precluded assessment of SPT regulation in the absence of ORM proteins.

In the current study, to advance our understanding of ORM-mediated sphingolipid biosynthesis, we generated *orm1 orm2* double mutants using CRISPR/Cas9. Loss of SPT regulation resulted in nonviable seeds with low oil content that accumulated high levels of ceramides. We mimicked this phenotype by removing the first transmembrane domain of LCB1, which is known to interact with ORM for SPT regulation (Han *et al.*, 2019). These studies also uncovered a single amino acid-deletion mutant of ORM1 that had severely altered membrane and organellar structures and that also hyperaccumulated ceramides. Using a yeast model, we showed that the deleted amino acid, which occurs in a position preceding the second membrane-spanning domain of ORM, strongly reduced the ORM-LCB1 interaction. This finding provides important information about the structural features of ORM and ORMDL proteins that are associated with their regulatory interaction with the LCB1 subunit of SPT.

RESULTS

ORMs are Essential for Plant Development

We designed two single guide RNAs (sgRNAs) to target regions in the coding sequence of each of the two Arabidopsis *ORM* genes (Figure 1A). We introduced these constructs into Arabidopsis via *Agrobacterium tumefaciens*-mediated transformation to

generate CRISPR/Cas9-induced knockouts of the *ORM1* and *ORM2* genes. We screened T_1 and T_2 transformants by restriction enzyme digestion of the PCR amplicons encompassing the *ORM1* and *ORM2* target sites to obtain homozygous lines with mutations in each gene. These lines were also verified by PCR to lack *Cas9* transgenes. These homozygous single mutants were visually indistinguishable from wild-type plants under optimal growth conditions (Figure 1B). The population of mutants obtained contained nucleotide deletions resulting in frameshifts and premature stop codons, as determined by PCR-restriction enzyme digestion and sequencing (Supplemental Figure 1). To obtain double knockout mutants, we crossed the *orm1*$^{-/-}$ and *orm2*$^{-/-}$ single mutants. No progeny with homozygous knockout mutations in both genes were obtained after analyzing 155 plants from the F_2 generation and 60 plants from the F_3 generation. To gain more insight into the basis for the apparent lethality associated with the double mutant, we performed viability staining on pollen from plants genotyped as *orm1*$^{+/-}$ *orm2*$^{+/-}$ (Supplemental Figure 2A). Nearly all of the pollen from these mutants was viable, similar to pollen from wild-type plants (Figure 1C and 1D), rather than 25% non-viability that would be expected for pollen lethality in this mutant.

Instead, a population of seeds from these plants had dark-colored seed coats and were severely wrinkled. This phenotype was observed for ~7% of seeds collected from the F_2 *orm1*$^{+/-}$ *orm2*$^{+/-}$ plants of *orm1*$^{-/-}$ and *orm2*$^{-/-}$ crosses, which is consistent with the expected 6.25% Mendelian ratio for the occurrence of homozygous double mutants. The remaining seeds were visually indistinguishable from wild-type seeds (Figure 1E and 1F). Of the seeds in these two populations, dark, wrinkled seeds did not germinate, whereas seeds with normal appearance showed no impairment in germination on solid sucrose-containing medium (Figure 1G and 1H) and soil. Strikingly, free ceramide concentrations in pooled abnormal seeds were ~40-fold higher than those in wild-type seeds and ~8-fold higher than in the normal appearing seed segregants from *orm1*$^{+/-}$*orm2*$^{+/-}$ plants (Figure 1I). We also observed a similar seed phenotype in *Atlcb1*$^{+/-}$ plants expressing a version of the LCB1 subunit of SPT lacking its first transmembrane domain (LCB1ΔTMD1) that is required for SPT-ORM regulatory interactions (Han *et al.*, 2019). In these experiments, the segregating seeds from

Atlcb1$^{+/-}$ plants expressing *LCB1ΔTMD1* included a population of shrunken, nonviable seeds with a 14-fold increase in ceramide levels relative to wild-type seeds (Figure 2).

We examined seeds from the *orm1*$^{-/-}$ and *orm2*$^{-/-}$ crosses and *LCB1ΔTMD1* in more detail to understand the basis for the loss of viability. The weight of mature nonviable, abnormal seeds was 80 to 90% lower than that of normal seed segregants from these lines (Figure 3E). Embryos dissected from the abnormal seeds had variable appearance ranging from cell clusters with undifferentiated appearance to embryo-like structures that were up to one-third the size of those from normal seeds (Figure 3 A-D). Underlying this phenotype, oil content of the abnormal seeds, as measured by the fatty acid content of purified triacylglycerols (TAG), was 85 to 90% lower than that of normal seed segregants (Figure 3F).

The most striking difference in fatty acid composition of TAG from the abnormal seeds was a reduction in the overall content of C20 and C22 very long-chain fatty acids derived from ER-localized elongation reactions. Notably, the fatty acids 20:2, 20:3, and 22:1 were not detectable in TAG from the abnormal seeds (Figure 3G).

Overall, these results indicate that ORMs are essential for the completion of a full lifecycle in Arabidopsis. Lethality due to the absence of ORM proteins is associated with the recovery of nonviable seeds with undeveloped embryos that accumulate excessive ceramide concentrations and have strongly reduced TAG levels. This was phenocopied in plants with deregulated SPT activity due to the loss of the transmembrane domain of LCB1 that abolishes ORM regulation of SPT (Han *et al.*, 2019). The identification of nearly the same phenotype in *ORM*-null mutants and LCB1-ΔTMD1 lines also indicated that the loss of seed viability is associated with the role of ORM proteins in sphingolipid metabolism, rather than other reported functions of ORM in Arabidopsis (Yang *et al.*, 2019).

The availability of progeny from *orm1*$^{-/-}$ and *orm2*$^{-/-}$ crosses also allowed us to assess the contributions of each *ORM* gene to the viability and growth of Arabidopsis plants. In addition to our inability to obtain homozygous double mutants for these genes, we observed that *orm1*$^{-/-}$ *orm2*$^{+/-}$ mutants were strongly dwarfed, with yellow leaves and senesced prior to flowering (Figure 4A). By contrast, *orm1*$^{+/-}$*orm2*$^{-/-}$ mutants had a distinct bushy phenotype, with increased leaf number compared to wild-type plants and

delayed flowering time (Figure 4B and 4C). Overall, these results revealed stronger growth phenotypes for the homozygous *ORM1* knockout in the *orm2*$^{+/-}$ background compared to the homozygous *ORM2* knockout in the *orm1*$^{+/-}$ background.

The *orm1*$^{\Delta met/\Delta met}$ *orm2*$^{-/-}$ Mutant does not Survive Beyond the Seedling Stage

Screening of gene-edited lines also revealed a mutant with an in-frame deletion of a single codon that resulted in a deletion of the methionine residue at amino acid 51 relative to the wild-type ORM1 (Figure 5B). This line also carried nucleotide deletions in *ORM2* that led to a frameshift and premature stop codon (Supplemental Figures 1 and 2B). Seedlings with the genotype *orm1*$^{\Delta met/\Delta met}$ *orm2*$^{+/-}$ showed a phenotype like wild type and the single mutants under normal growth conditions (Figure 5A).

However, we could only recover plants of the genotype *orm1*$^{\Delta met/\Delta met}$ *orm2*$^{-/-}$ in solid medium supplemented with sucrose. The resulting seedlings were severely dwarfed and had a proliferation of small, deformed chlorotic leaves. These plants persisted in a visually viable state for 20-25 days after planting but did not progress beyond the seedling stage, indicating that the *orm1*$^{\Delta met/\Delta met}$ *orm2*$^{-/-}$ mutation is seedling lethal (Figure 5A and 5C-5F). Complementation of this mutant with the Arabidopsis *ORM1* cDNA under the control of its native promoter was sufficient to rescue the seedling lethality and recover fertile plants, although many of the independent complemented mutant lines were smaller than wild-type plants, which is similar to the phenotype of *orm1*$^{+/-}$*orm2*$^{-/-}$ plants, as described above (Supplemental Figure 3).

The *orm1*$^{\Delta met/\Delta met}$ *orm2*$^{-/-}$ Mutant Hyperaccumulates Selected Sphingolipids

Based on the finding that downregulating *ORM* expression triggers sphingolipid accumulation (Breslow *et al.*, 2010; Kimberlin *et al.*, 2016; Li *et al.*, 2016), we conducted extensive sphingolipidomic profiling of our gene-edited mutants from seedlings grown on sucrose medium at 12-15 days after planting. The *orm1*$^{\Delta met/\Delta met}$ *orm2*$^{-/-}$ mutant accumulated 3.7-fold more sphingolipids than wild-type seedlings (Figure 6A). No significant differences in the levels of free long-chain bases (LCB), ceramides with non-hydroxylated fatty acids (Cer), or other sphingolipid classes were detected in the

orm1$^{-/-}$, *orm2*$^{-/-}$, or *orm1*$^{\Delta met/\Delta met}$ *orm2*$^{+/-}$ mutants compared to wild-type plants (Figure 6B-6E and 6G-6I). In strong contrast, *orm1*$^{\Delta met/\Delta met}$ *orm2*$^{-/-}$ seedlings showed heightened accumulation of LCB (5-fold), Cer (90-fold) and ceramides with hydroxylated fatty acids (hCer; 12-fold) compared to wild-type seedlings of similar age (Figure 6B-6D; Supplemental Figure 4).

Although no changes were detected in GlcCer concentrations, the levels of glucosylceramides (GlcCer) containing non-hydroxylated fatty acids (nhGlcCer), not typically found in abundance in Arabidopsis, were 13-fold higher in *orm1*$^{\Delta met/\Delta met}$ *orm2*$^{-/-}$ seedlings versus wild-type seedlings (Figure 6E, 6G; Supplemental Figures 5 and 6). Glycosylinositolphosphoceramide (GIPC) levels increased by 48% in the *orm1*$^{\Delta met/\Delta met}$ *orm2*$^{-/-}$ mutant compared to wild-type seedlings (Figure 6F; Supplemental Figure 7). The LCB composition of the single mutants and *orm1*$^{\Delta met/\Delta met}$ *orm2*$^{+/-}$ did not change significantly compared to wild type (Figure 7A and 7B). However, in *orm1*$^{\Delta met/\Delta met}$ *orm2*$^{-/-}$, the levels of free and phosphorylated forms of d18:0 were the most strongly increased, with lesser increases in the amounts of t18:0 and t18:1 free and phosphorylated species (Figure 7A and 7B).

Cer profiles of the single mutants were similar to those of the wild type (Figure 7C-7E). By contrast, the *orm1*$^{\Delta met/\Delta met}$ *orm2*$^{+/-}$ mutant had increased amounts of Cer with C16 fatty acids relative to wild type and single mutant plants (Figure 7F). This phenotype was more accentuated in *orm1*$^{\Delta met/\Delta met}$ *orm2*$^{-/-}$ seedlings, which primarily accumulated Cer species with C16 fatty acids linked to the dihydroxy LCB d18:0 and d18:1 (Figure 7G). Increased amounts of Cer with C22, C24 and C26 fatty acids as well as atypical C18 and C20 fatty acid-containing species were also detected in *orm1*$^{\Delta met/\Delta met}$ *orm2*$^{-/-}$ seedlings relative to wild-type plants and mutants of either *ORM* gene (Figure 7G). Overall, the primary change in the composition of all sphingolipid classes, especially Cer, hCer and nhGlcCer, in the in *orm1*$^{\Delta met/\Delta met}$ *orm2*$^{-/-}$ seedlings was the change in the total and/or relative amounts of those containing C16 fatty acids bound to dihydroxy LCB, which are derived from the LOH2 ceramide synthase (Figure 7G; Supplemental Figures 4 and 6) (Markham *et al.*, 2011; Ternes *et al.*, 2011; Luttgeharm *et al.*, 2015a). The *orm1*$^{\Delta met/\Delta met}$ *orm2*$^{-/-}$ plants also contained aberrant forms of hCer and

GIPCs with currently undefined structures based on LC-MS ionization as well as Cer with the LCB deoxy-sphinganine (DoxSA), which is derived from the condensation of alanine, rather than serine, to palmitoyl-CoA by SPT (Figure 6I). In addition, the concentration of inositolphosphorylceramides (IPCs), the precursors of GIPCs, increased nearly 12-fold in small *orm1*$^{met/met}$ *orm2*$^{-/-}$ seedlings vs. the wild type (Figure 6H).

Overall, these findings are consistent with the notion that SPT regulation by the *orm1*^{met}-encoded polypeptide is deficient and that the flux of excess LCB occurs through the LOH2 ceramide synthase to produce Cer backbones with C16 fatty acids and dihydroxy LCB, a portion of which are channeled to GIPCs but accumulate as IPC intermediates.

The Integrity of Cellular Component is Compromised in the *orm1*$^{met/met}$ *orm2*$^{-/-}$ Mutant

Given that sphingolipids are abundant endomembrane and plasma membrane components that contribute to vesicular trafficking, we used transmission electron microscopy (TEM) to evaluate the subcellular phenotypes associated with enhanced sphingolipid accumulation in 10-day-old *orm1*$^{met/met}$ *orm2*$^{-/-}$ seedlings relative to wild-type seedlings of the same age. Mesophyll cells from wild-type seedlings showed large vacuoles with turgor pressure pushing organelles to the periphery (Figure 8A). Chloroplasts of wild-type cells had the typical oval shape and well-defined thylakoid membranes (Figure 8A and 8B). By contrast, the *orm1*$^{met/met}$ *orm2*$^{-/-}$ mutant cells displayed a lack of vacuolar turgor (Figure 8D). In addition, chloroplasts of *orm1*$^{met/met}$ *orm2*$^{-/-}$ cells were round and showed marked disintegration of thylakoids and highly abundant osmiophilic structures that resemble plastoglobuli (Figure 8C-8F).

Notably, increased vesicle numbers were observed around the ER network in *orm1*$^{met/met}$ *orm2*$^{-/-}$ cells (Figure 8F). Furthermore, electrodense material and double membrane vesicles consistent with autophagosomes were detected inside the vacuoles of these cells. Moreover, entire chloroplasts were engulfed and appeared to be in the

process of degradation (Figure 8G and 8H). Despite these large defects, Golgi stacks were detectable in *orm1*$^{\Delta met/\Delta met}$ *orm2*$^{-/-}$ cells (Figure 8I).

Genes for Ceramide Synthases, LCB Kinase, and LCB Phosphate Lyase are Upregulated in the *orm1*$^{\Delta met/\Delta met}$ *orm2*$^{-/-}$ Mutant

Given the increased concentrations of most sphingolipid classes in *orm1*$^{\Delta met/\Delta met}$ *orm2*$^{-/-}$, we examined the expression of genes in 12-day-old seedlings for key sphingolipid biosynthetic and catabolic enzymes, including the SPT-associated polypeptides LCB1 and ssSPTa, ceramide synthases (LOH1, LOH2, and LOH3), sphingosine kinases (SPHK1 and SPHK2), and the LCB catabolic enzyme LCB-phosphate lyase (or DPL1). No significant differences were detected in the expression of genes for LCB1, ssSPTa, or LOH1 in any mutant analyzed (Supplemental Figure 8A-8C). However, consistent with the increased amounts of ceramides in *orm1*$^{\Delta met/\Delta met}$ *orm2*$^{-/-}$, the ceramide synthase gene *LOH2* showed a ~2.5-fold increase in expression and the ceramide synthase gene *LOH3* showed a ~2-fold increase in *orm1*$^{\Delta met/\Delta met}$ *orm2*$^{-/-}$ plants compared to wild type and the other mutants examined (Figure 9A and 9B). Most notably, the expression of the key sphingolipid catabolism-associated genes *SPHK2* and *DPL1* increased by ~6 to 7-fold respectively, in *orm1*$^{\Delta met/\Delta met}$ *orm2*$^{-/-}$ plants relative to the wild type and other *ORM* mutants (Figure 9C and 9D). This result is consistent with the notion that the induction of LCB catabolism is one route (in addition to ceramide biosynthesis) for the mitigation of unregulated LCB production in the *orm1*$^{\Delta met/\Delta met}$ *orm2*$^{-/-}$ mutant.

Defense and Senescence Genes are Upregulated in the *orm1*$^{\Delta met/\Delta met}$ *orm2*$^{-/-}$ Mutant

The accumulation of ceramides has been linked to the activation of signaling pathways that lead to PCD (Liang *et al.*, 2003; Bi *et al.*, 2014). To examine whether the high amounts of ceramides in *orm1*$^{\Delta met/\Delta met}$ *orm2*$^{-/-}$ activate PCD, we performed qPCR of marker genes using RNA extracted from 12-day-old seedlings. The expression of the pathogenesis-related genes (*PR-2, PRXC, FMO, PR3*) was significantly higher in *orm1*$^{\Delta met/\Delta met}$ *orm2*$^{-/-}$ compared to wild type and the other mutants (Figure 9E-9G,

Supplemental Figure 8E). A similar expression pattern was also observed for the senescence-related gene *SAG13* (Figure 9H).

ORM1Δ^{met} Fails to Interact with LCB1 to Suppress SPT Activity

Our results clearly show that ORM1 lacking Met51 is strongly impaired in repressing SPT activity. This amino acid is located in the ER luminal domain immediately adjacent to the second transmembrane domain of ORM1 (Supplemental Figure 9). We hypothesized that, without this amino acid, the conformation of the second transmembrane domain of ORM1 is altered such that the interaction with LCB1 for the repression of SPT activity is disrupted. To better understand this regulatory mechanism, we stably expressed the Arabidopsis ORM1Δ^{met} mutant protein in a *S. cerevisiae* mutant background in which AtLCB1, AtLCB2, and AtssSPTa replaced the corresponding yeast SPT-associated polypeptides, as confirmed by immunoblotting (Figure 10A). We assessed *in vivo* SPT activity by measuring the DoxSA produced when expressing AtLCB1^{C144W} (Figure 10B). Deoxy-LCBs cannot be phosphorylated/degraded and are used as a readout for *in situ* SPT activity (Gable et al., 2010; Kimberlin et al. 2016). When expressed in this yeast background, wild-type Arabidopsis ORM1 was able to suppress DoxSA production, which is consistent with its function as a negative regulator of SPT activity. By contrast, DoxSA concentrations in ORM1Δ^{met}-expressing cells were similar to those in vector control cells lacking ORM1, which is consistent with a lack of repressed SPT activity.

ORMs interact with the first transmembrane domain of LCB1 to repress SPT activity in *S. cerevisiae* (Han *et al.*, 2019), although the structural components of ORM associated with this interaction have not been defined. To test whether ORM1Δ^{met} physically interacts with AtLCB1, as does wild-type ORM1, we performed co-immunoprecipitation of FLAG-tagged AtLCB1 with solubilized microsomes from yeast cells expressing Myc-AtLCB2a, HA-ssSPTa and HA-ORM1 or HA-ORM1Δ^{met}. Pull-downs of AtLCB1 resulted in co-immunoprecipitation of AtLCB2a and AtORM1, but not ELO3, an ER protein that does not interact with SPT. By contrast, only trace amounts of HA-ORM1Δ^{met} were detected in the AtLCB1 pull-downs (Figure 10C).

This finding indicates that Met51 is critical for the ORM-LCB1 physical interaction to regulate SPT activity. To determine whether the impaired ORM-LCB1 interaction is due to gross or subtle alterations in the secondary structure of ORM induced by the Met51 deletion, we compared the membrane topology of ORM1 and ORM1Δ^{met}. We inserted glycosylation cassettes into the two predicted ER luminal loops (at amino acids 46 and 121) and into the cytosolic loop between the second and third transmembrane domains (at amino acid 82) and expressed the proteins in *S. cerevisiae* along with reconstituted Arabidopsis SPT. The analysis showed that the cassettes in the predicted luminal domains were glycosylated while the cassette in the predicted cytosolic domain was not (Figure 10D). Thus, we conclude that ORM1 with the Met51 deletion retains the topology of wild-type ORM1.

DISCUSSION

Our findings identified the essential role of sphingolipid biosynthetic regulation at the level of SPT for seed viability, which was previously unclear due to the lack of complete knockout mutants for *ORM* genes in plants. We showed that *orm1*$^{-/-}$ *orm2*$^{-/-}$ seeds have impaired embryo development accompanied by hyperaccumulation of the cytotoxic sphingolipid biosynthetic intermediates ceramides. Strongly enhanced ceramide accumulation was also observed in the *S. cerevisiae orm1Δ/orm2Δ* mutant (Breslow *et al.*, 2010; Han *et al.*, 2010) and recently in *Ormdl1/3* mutant mice (Clarke *et al.,* 2019). We also confirmed that impaired seed viability in the mutant is due solely to the function of ORMs in SPT regulation, rather than other ascribed ORM functions (Yang *et al.*, 2019). This was achieved by mimicking this phenotype by removing the first transmembrane domain of LCB1, which is required for ORM binding to SPT (Han *et al.*, 2019). Furthermore, through gene editing, we recovered the *orm1*$\Delta^{met/\Delta met}$ *orm2*$^{-/-}$ mutant, which expresses an ORM1 structural variant that is strongly compromised in the regulation of SPT activity. This mutant provided valuable insight into cellular responses to unchecked sphingolipid biosynthesis. These responses include compromised organellar structures, the induction of catabolic genes to maintain sphingolipid

homeostasis, and clues about the structural requirements of ORM for interaction with LCB1.

Our findings emphasize that the full significance of ORMs to plant viability can only be assessed by complete knockout of the corresponding genes. By contrast, Arabidopsis *ORM*-suppressed plants previously generated by RNAi or amiRNA methods were fully viable, although the response to bacterial pathogens was altered in these plants and early senescence was observed with the most extreme suppression of *ORM* expression (Kimberlin *et al.*, 2016; Li *et al.*, 2016). Similar to our findings, a recent report revealed the inability to recover mice lacking all three *ORMDL* genes (Clarke *et al.,* 2019). However, we were able to more precisely determine that lethality occurs during seed development rather than during gametogenesis. This finding contrasts with those from previous studies of plants with strongly reduced sphingolipid biosynthetic capacity due to impaired SPT activity (Dietrich *et al.*, 2008; Teng *et al.*, 2008; Kimberlin *et al.*, 2013). In these mutants, pollen is defective in endomembrane formation and is unable to complete maturation. Sphingolipids accumulate to exceptionally high levels in Arabidopsis pollen relative to leaves (Luttgeharm *et al.*, 2015b; Ischebeck, 2016). As such, it is likely that pollen is able to tolerate unregulated sphingolipid synthesis that results from complete *ORM* knockout.

The mechanism underlying the loss of seed viability from unregulated SPT activity in *orm1*$^{-/-}$ *orm2*$^{-/-}$ and *orm1*$^{met/met}$ *orm2*$^{-/-}$ mutants likely involves a combination of the functions of sphingolipids as major structural components of the endomembrane and as bioactive mediators of cellular activities such as PCD that lead to aberrant embryo development. As shown in *orm1*$^{met/met}$ *orm2*$^{-/-}$ seedlings, strong upregulation of sphingolipid biosynthesis results in large alterations in membrane and organellar structures in plant cells (Figure 8). These seedlings appear to have defects in ER function, as indicated by the relative reduction in the total content of very long-chain fatty acids in the abnormal seeds from the progeny of *orm1*$^{-/-}$ and *orm2*$^{-/-}$ crosses and *LCB1ΔTMD1* transgenic lines (Figure 3G). These fatty acids are formed by ER-localized enzymes including the *FAE1*-encoded β-ketoacyl-CoA synthase. The hyperaccumulation of ceramides in these seeds also likely triggers PCD in embryonic

cells, as indicated by the enhanced expression of PCD-related genes in *orm1*$^{\Delta met/\Delta met}$ *orm2*$^{-/-}$ seedlings (Figure 9E-9G and Supplemental Figure 8E).

Among the gene-edited *ORM* variants identified in our studies was a mutant that contained an in-frame deletion of Met51 combined with a homozygous knockout of *ORM2* (*orm1*$^{\Delta met/\Delta met}$ *orm2*$^{-/-}$). Seeds from this mutant were viable, in contrast to *orm1*$^{-/-}$*orm2*$^{-/-}$; however, the plants did not advance beyond the seedling stage and had strong developmental defects. Like the *orm1*$^{-/-}$*orm2*$^{-/-}$ seeds, the *orm1*$^{\Delta met/\Delta met}$ *orm2*$^{-/-}$ seedlings hyperaccumulated ceramides with C16 fatty acids. These seedlings also accumulated aberrant sphingolipids including DoxSA-containing ceramides, GlcCer containing non-hydroxylated fatty acids, and IPCs, all of which were nearly absent from wild-type seedlings. Cells from the *orm1*$^{\Delta met/\Delta met}$ *orm2*$^{-/-}$ seedlings displayed gross defects in membrane and organellar structures as well as apparent autophagosome-like structures. The early cell death displayed by the *orm1*$^{\Delta met/\Delta met}$ *orm2*$^{-/-}$ seedlings can be attributed to the activation of PCD pathways, as indicated by the high transcript levels of pathogenesis- and senescence- related genes that have been shown to be activated by the accumulation of LCB and ceramides.

Notably, Met51 is predicted to occur at a position that is adjacent to the second transmembrane domain of ORMs but is not a conserved residue across eukaryotic ORM or ORMDL proteins (Supplemental Figure 9). Using yeast mutants containing the Arabidopsis SPT complex, we determined that the ORM1 Met51 mutant has greatly reduced interaction with Arabidopsis LCB1, which is required for ORM-induced suppression of SPT activity. Given that Met51 is not conserved in eukaryotes, it is likely that LCB1 does not directly interact with this residue. Instead, the lack of this amino acid likely produces a conformational change at the second transmembrane domain of ORM that impedes its regulatory interaction with the first transmembrane domain of LCB1. The maintenance of the topology of ORM1$^{\Delta Met51}$ in microsomal membranes was verified by Endo H digestion studies using the mutant ORM1 protein carrying glycosylation cassettes. To date, no residues or structural features in ORMs have been identified that are associated with their interaction with the LCB1/LCB2 heterodimer of SPT. Our findings point to the possible interaction of the first transmembrane domain of LCB1 with

the second transmembrane domain of ORM as the basis for SPT regulation. Additional structural studies are required to fully elucidate these potential regulatory interactions between ORM and LCB1.

The use of gene editing also allowed us to assess the redundancy of *ORM1* and *ORM2*. Notably, single mutants and progeny from the crosses that genotype as *orm1*$^{+/-}$ *orm2*$^{+/-}$ had an appearance similar to wild-type plants under normal conditions. However, *orm1*$^{-/-}$ *orm2*$^{+/-}$ seedlings displayed early senescence and did not flower (Figure 4A). By comparison, *orm1*$^{+/-}$ *orm2*$^{-/-}$ plants were fertile but were strongly dwarfed and had delayed flowering compared to wild type and *orm1*$^{+/-}$ *orm2*$^{+/-}$ plants (Figure 4B and 4C). Perhaps the stronger phenotype associated with the complete ORM1 knockout in the ORM2 heterozygous background reflects the finding that *ORM1* is more highly expressed than *ORM2* throughout the plant except in pollen (Kimberlin *et al.*, 2016). The normal appearance of mutants genotyped as *ORM1/orm2*$^{-/-}$ and *orm1*$^{-/-}$*/ORM2* suggests that *ORM1* and *ORM2* are functionally redundant, despite the phenotypic differences observed in *orm1*$^{-/-}$ *orm2*$^{+/-}$ and *orm1*$^{+/-}$ *orm2*$^{-/-}$ seedlings. However, we did observe that *orm1*$^{+/-}$ *orm2*$^{-/-}$ plants have a highly bushed appearance and are strongly delayed in flowering (>80 days to flowering) (Figure 4D), pointing to a meristem defect (Tantikanjana *et al.* 2001). This phenotype requires further investigation, but it suggests that ORM2 contributes more strongly to meristem function than ORM1, perhaps due to cell-type-specific differences in the expression of the *ORM* genes or to a non-sphingolipid function of ORM proteins.

Our results also revealed transcriptional mechanisms for maintaining sphingolipid homeostasis upon the enhanced production of long-chain bases in the *orm1*$^{met/met}$ *orm2*$^{-/-}$ mutant. *LOH2* and *LOH3* (encoding the functionally distinct ceramide synthases LCB kinases) and *DPL1* (encoding the last step in long-chain base degradation) were transcriptionally upregulated in the mutant. Notably, upregulating *LOH2* expression was associated with the preponderance of ceramides containing C16 fatty acids and dihydroxy long-chain bases (the principal products of LOH2 ceramide synthase activity) in free ceramides and glucosylceramides, including non-hydroxylated glucosylceramides, which accumulated in *orm1*$^{met/met}$ *orm2*$^{-/-}$ seedlings but were

detected at only low concentrations in wild type and *ORM1* and *ORM2* single mutants. These findings are consistent with our previous report that LOH2 activity is upregulated in Arabidopsis *ORM* RNAi plants, presumably as a pathway for reducing cytotoxicity of free long-chain bases and ceramides (which are metabolized to glucosylceramides) (Kimberlin *et al.*, 2016). No changes were detected in *LCB1* or *ssSPTa* transcript levels in the *orm1*$^{\Delta met/\Delta met}$ *orm2*$^{-/-}$ mutant, indicating that the transcriptional regulation of genes for SPT complex proteins is not a pathway for maintaining sphingolipid homeostasis in response to deregulated long-chain base biosynthesis. Instead, the expression of genes involved in the catabolism of LCBs increased ~six- to seven-fold (*SPHK2* and *DPL1*) in this mutant, suggesting that an unknown mechanism is activated in response to increased ceramide and/or LCB levels.

Our overall findings about the metabolic and developmental defects associated with the deregulation of SPT by disrupting ORM genes or removing the first transmembrane domain of LCB1 are schematically summarized in Figure 11. These sphingolipid-related regulatory processes identified in Arabidopsis are likely found in other plant species due to the conservation of sphingolipid metabolic enzymes in the plant kingdom. Still unanswered is how ORM interactions with LCB1 are regulated in response to perturbations in intracellular sphingolipid levels or abiotic and biotic stresses (e.g., bacterial and fungal pathogenesis). Similar to mammalian ORMDLs, plant ORMs lack the serine-rich N-terminal extension found in *S. cerevisiae* ORMs, which is phosphorylated or dephosphorylated in response to intracellular sphingolipid levels to mediate ORM-LCB1 interactions (Breslow *et al.*, 2010; Han *et al.*, 2010). Mammalian ORMDLs have recently been shown to bind ceramides directly, which affects the interactions of ORMs with LCB1 (Davis *et al.,* 2019). A similar regulatory mechanism might occur in plants. In this regard, we previously speculated that LOH2-derived ceramides or glycosphingolipids enriched in dihydroxy LCBs and C16 fatty acids likely provide minimal SPT regulation relative to those containing trihydroxy LCBs and very long-chain fatty acids based on the hyperaccumulation of sphingolipids found in *sbh1 sbh2* mutants and *LOH2*-overexpressing plants (Chen *et al.*, 2008; Luttgeharm *et al.*, 2015a). Still, how ORMs reversibly regulate SPT activity in response to cellular sphingolipid requirements remains an outstanding question in plants.

METHODS

Plant Materials and Growth Conditions

Arabidopsis thaliana Columbia-0 (Col-0) was used as the wild-type reference in this study. Arabidopsis seedlings were grown on Murashige and Skoog (MS) medium supplemented with 1% sucrose and 0.8% agar (pH 5.7) with 16 h light (100μmol/ m^{-2} s^{-1}) 8 h dark conditions at 22°C. The light source for growth chamber-grown seedlings was supplied by standard wide-spectrum fluorescent bulbs type F32/841/ECO 32 watt (maximum intensity 480-570 nm). For Arabidopsis plants in soil, seeds were sown, and after 2 days of stratification at 4°C, plants were grown at 22°C with 16 h light (100 μmol/ m^{-2} s^{-1}) 8 h dark. The light source for these plants came from wide-spectrum fluorescent bulbs of type F32/841/ECO 32 watt and/or F72/T12/CW/VHO 160 watt and F96/T12/CW/VHO215 215 watt (maximum intensity 480-570 nm).

Generation of CRISPR/Cas9 ORM Mutants

For CRISPR/Cas9-mediated gene editing of *ORM1* and *ORM2*, designed target sites (Figure 1A) were fused with a single guide RNA (sgRNA) and expressed under the control of the U6 promoter. The egg cell-specific *EC1* promoter was used to drive *Cas9* expression as previously reported (Wang *et al.*, 2015). In short, *Bsa*I sites were incorporated by PCR into the *ORM* target sequences (Primers P1-P4; Supplemental Table 1). The purified PCR products were digested with *Bsa*I and ligated to the *Bsa*I-linearized binary vector pHEE401E. The final CRISPR/Cas9 binary vector was electroporated into *Agrobacterium* strain GV3101 and then transformed into Arabidopsis Col-0 wild-type plants via the floral dip method (Clough and Bent, 1998). The seeds were screened for hygromycin resistance on MS plates containing 25 mg/L hygromycin. For genotyping, fragments including the target regions of *ORM1* and *ORM2* were amplified by PCR from the genomic DNA of transgenic plants (primers P5-P8; Supplemental Table 1). Amplicons were digested with the restriction enzyme *Bsl*I (*ORM1*) and *Dra*III (*ORM2*). The specific indels were identified by DNA sequencing. To analyze for non-transgenic plants, progeny of hygromycin selected and confirmed

homozygous (CRISPR/Cas9 mutation) T_1 plants were sown directly on soil without hygromycin selection. These plants were then screened by PCR (P9+P10; Supplemental Table 1) for the lack of the *Cas9* gene with the presence of the CRISPR mutation, in the T_2 generation. The plants lacking *Cas9* but containing the CRISPR mutation were kept and used for further studies as mutated but non-transgenic lines.

Genetic Complementation of *orm1□$^{met/□met}$ orm2$^{-/-}$*

For genetic complementation of the mutant *orm1□$^{met/□met}$ orm2$^{-/-}$, ORM1* cDNA was synthesized with included silent mutations of the *ORM1* gRNA target sequence to mitigate possible editing of the transgene. The cDNA was amplified by overlapping PCR and cloned into the *Eco*RI and *Xba*I sites of binary vector pBinGlyRed3 under the control of the native *ORM1* promoter 600 bp region upstream of the *ORM1* start codon (primers P11-P16; Supplemental Table 1). *orm1□$^{met/□met}$ orm2$^{+/-}$* plants were transformed with the pBinGlyRed3-*ORM1* construct by the floral dip method (Clough and Bent, 1998). Transformants were selected based on DsRed fluorescence and genotyped. Mutation was confirmed by sequencing.

Generation of the *LCB1□TMD1* Mutant

LCB1□TMD1 was generated by deleting 63 nucleotides corresponding to the first transmembrane domain of At*LCB1* (nucleotide 95-157). *LCB1□TMD1* under the control of the LCB1 native promoter was cloned into the pBinGlyRed3 binary vector, which was transformed into *Agrobacterium tumefaciens* GV3101 by electroporation. Heterozygous LCB1/lcb1-KO mutants (SALK_077745) were transformed by the floral dip method (Clough and Bent, 1998).

Pollen Staining

Anthers of mature plants were isolated and smeared on a glass slide. The pollen was stained using Alexander staining method (Alexander, 1969) for 1 h at 25°C. Pollen imaging was performed using the EVOS FL Auto Cell Imaging System.

Sphingolipid Extraction and Analysis

Sphingolipids were extracted as described in (Markham and Jaworski, 2007). Briefly, 12 to 15-day-old Arabidopsis seedlings grown on solid medium were collected from independent plates for each biological replicate. The seedlings were lyophilized and 10-30 mg of tissue was homogenized and extracted with isopropanol/heptane/water (55:20:25 v/v/v). We used one to four mg of plant material for each biological replicate for sphingolipid analysis from seeds. Internal standards for the different sphingolipid classes were added. The supernatants were dried and de-esterified with methylamine in ethanol/water (70:30 v/v). The lipid extract was re-suspended in THF/methanol/water (5:2:5 v/v/v) containing 0.1% formic acid. The sphingolipid species were analyzed using a Shimadzu Prominence ultra-performance liquid chromatography system and a 4000 QTRAP mass spectrometer (AB SCIEX). Data analysis and quantification were performed using the software Analyst 1.5 and Multiquant 2.1 as described (Markham and Jaworski, 2007; Kimberlin *et al.*, 2013; Davis *et al.*, 2020).

Lipid Extraction Analysis

To quantify the TAG content, lipids were extracted from ~1 mg of seeds using a method based on that of Bligh and Dyer (Bligh and Dyer, 1959). Seeds were ground using a glass rod in 13 × 100-mm glass screw cap tubes with 3 mL methanol:chloroform (2:1 v/v). Triheptadecanoin (17:0-TAG) was added to the seeds as an internal standard prior to extraction. After 1 h incubation at 25°C, 1 mL of chloroform and 1.9 mL of water were added. The solution was mixed thoroughly and centrifuged at 400•*g* for 10 min. The lower organic phase containing total lipids was transferred to a new glass tube and solvent evaporated under a N_2 stream with heating at 40°C. The sample was redissolved in 1 mL of heptane and loaded onto a solid phase extraction column (Supelco Supelclean LC-Si SPE column; Sigma-Aldrich) pre-equilibrated with heptane. A purified TAG fraction was eluted from the column and converted to fatty acid methyl esters, which were analyzed by gas chromatography as previously described (Zhu *et al.*, 2016). TAG fatty acid content was quantified relative to 17:0 fatty acid methyl ester from the internal standard.

RNA Isolation and Quantitative RT-PCR

RNA was extracted from 12 to 15-day-old Arabidopsis seedlings grown on solid MS medium. Each replicate corresponds to pooled seedlings from independent plates. RNA extraction was performed using an RNeasy Kit (Qiagen) according to the manufacturer's protocol. The isolated RNA (1 μg) was treated with DNase I (Invitrogen). cDNA conversion was performed with a RevertAid cDNA synthesis kit (Thermo Fisher). SYBR Green was used as the fluorophore in a qPCR supermix (Qiagen). *PP2AA3* and *UBIQUITIN* (*UBQ*) were used as internal reference genes. qPCR was performed using a Bio-Rad MyiQ iCycler qPCR instrument. The thermal cycling conditions were an initial step of 95°C for 10 min followed by 45 cycles at 95°C for 15 s, 60°C for 30 s and 72°C for 30 s. Primers used in this study are listed in Supplemental Table 1.

Electron Microscopy

Ten-day-old wild-type and *orm1*$^{met/met}$ *orm2*$^{-/-}$ seedlings were used for Transmission Electron Microscopy (TEM). The samples were cut and fixed with 2.5% glutaraldehyde (v/v), 2.0% paraformaldehyde in 0.1 M cacodylate buffer. The samples were subjected to post fixation with 1% osmium tetroxide in 0.1 M cacodylate buffer, dehydrated with ethanol and acetone, and embedded with a Spurr's Embedding Kit. Ultra-thin sections (100 nm) were cut and stained with uranyl acetate and lead citrate. Samples were imaged on a Hitachi H7500 TEM at an accelerating voltage of 80 kV.

Yeast Cell Growth and Expression Plasmids

Saccharomyces cerevisiae strain TDY9113 (Mata *tsc3*Δ:NAT*lcb1*Δ:KAN *ura3 leu2 lys2 trp1*Δ) lacking endogenous SPT was used for the expression of Arabidopsis SPT subunits and ORM proteins as described in (Kimberlin *et al.*, 2016). For deoxy-sphinganine (DoxSA) quantification, yeast strain TDY9113 expressing AtLCB1^{C144W} was grown in 1.5% galactose and 0.5% glucose supplemented with 40 mM alanine. Plasmids for the expression of AtLCB1-FLAG, Myc-AtLCB2a, and HA-AtssSPTa in yeast were as described (Kimberlin *et al.*, 2013) and for HA-AtORM1 as described (Kimberlin *et al.*, 2016). AtLCB1^{C144W} was generated by QuikChange mutagenesis (Agilent Technologies) and confirmed by sequencing. The open reading frame of ORM1Δ^{met51} was amplified by PCR and inserted into pPR3-N (Dualsystems Biotech) for

expression with an N-terminal HA tag. LCB and DoxSA quantification were performed as previously described (Kimberlin *et al.*, 2016).

Immunoprecipitation

Microsomal membrane proteins were prepared from yeast cells expressing FLAG-tagged AtLCB1, Myc-tagged AtLCB2a, HA-tagged AtssSPTa, and HA-tagged AtORM1 or AtORM1$_{\Delta}^{met}$. Microsomal membrane proteins were solubilized in 1.5% digitonin at 4°C for 2.5 h and incubated with Flag-beads (Sigma-Aldrich) overnight. The bound proteins were eluted in immunoprecipitation buffer (50 mM HEPES-KOH, pH 6.8, 150 mM potassium acetate, 2 mM magnesium acetate, 1 mM calcium chloride, and 15% glycerol) containing 0.25% digitonin and 200 μg/mL FLAG peptide, resolved on a 4% to 12% BisTris NuPAGE gel (Invitrogen), and detected by immunoblotting with anti-HA (Covance; 1:5,000 dilution), anti-Myc (Sigma-Aldrich; 1:3,000 dilution), and anti-FLAG (GenScript; 1:5,000 dilution) antibodies.

Membrane Topology Mapping of ORM1$_{\Delta}^{met}$

ORM or ORM1$_{\Delta}^{met51}$-encoding synthetic cDNAs with an in-frame glycosylation cassette (GC) inserted after codon 46, 82 or 121 were synthesized by GenScript (NJ, USA) and ligated into pPR3-N for expression with an N-terminal HA tag. The HA-ORM1-GC-tagged proteins were expressed (along with AtLCB1-FLAG, MYC-AtLCB2a, and HA-AtssSPTa) in yeast strain TDY9113. Isolation of microsomal proteins, digestion with Endo H, and immunodetection of the AtORM1 proteins were performed as previously described (Kimberlin *et al.*, 2016).

Statistical Analyses

Two-tailed Student's *t* test was performed to evaluate statistically significant differences compared to the control (wild-type). One-way ANOVA followed by Tukey's test was used to determine the differences among the five genotypes for a given variable. The values $P < 0.05$ were considered statistically significant. The statistical analyses were done using GraphPad Prism 8.3.0. T-test and ANOVA results are shown in Supplemental Data Set 1.

Accession Numbers

Accession numbers for the genes studied in this work are: *ORM1* (At1G01230), *ORM2* (At5g42000), *LCB1 (*At4g36480), *ssSPTa* (At1g06515), *LOH1* (At3g25540), *LOH2* (At3g19260), *LOH3* (At1g13580), *SPHK1* (At4g21540), *SPHK2* (At2g46090), *DPL1* (At1g27980), *PP2AA3* (At1g13320), *PRXC* (At3g49120), *PR2* (At3g57260), *PR3* (At3g12500), *FMO* (At1g19250), *SAG13* (At2g29350), and *UBQ* (At5g25760).

Supplemental Data

Supplemental Figure 1. Predicted Protein Sequences of ORMs in the CRISPR/Cas9 Mutants.

Supplemental Figure 2. PCR/Digestion-based Genotyping of CRISPR/Cas9 *ORM* Mutants.

Supplemental Figure 3. Complementation of *orm1*$^{met/met}$ *orm2*$^{-/-}$.

Supplemental Figure 4. Ceramide Compositions with Hydroxylated Fatty Acids in *ORM* Mutants.

Supplemental Figure 5. Glucosylceramide Compositions in *ORM* Mutants.

Supplemental Figure 6. Composition of Glucosylceramides Containing Non-Hydroxylated Fatty Acids in *ORM* Mutants.

Supplemental Figure 7. Glycosylinositolphosphoceramide Compositions in *ORM* Mutants.

Supplemental Figure 8. Expression of Genes Associated with Sphingolipid Biosynthetic and Catabolic Pathways and Pathogenesis.

Supplemental Figure 9. Amino Acid Sequence Alignment of ORM Proteins.

Supplemental Table 1. Primer Sequences Used for Cloning, RT-PCR, qPCR, and Genotyping.

Supplemental Data Set 1. T-tests and ANOVA Results.

ACKNOWLEDGEMENTS

We thank Jaydeeo Kolape for technical assistance and Jules Russ for the TEM sample preparation at the Microscopy Core Facility in the Center for Biotechnology at University of Nebraska-Lincoln. This work was supported by a National Science Foundation grant MCB 1818297 to EBC, TMD and JEM. AGS acknowledges the funding from the Mexican National Council of Science and Technology (CONACyT).

AUTHOR CONTRIBUTIONS

AGS, GH, TMD and EBC designed the study; AGS, GH, LG, YL, REC and JEM performed the experiments and analyzed the data along with GH, TMD, and EBC; AGS, GH, TMD, and EBC wrote the manuscript.

REFERENCES

Alden, K.P., Dhondt-Cordelier, S., McDonald, K.L., Reape, T.J., Ng, C.K., McCabe, P.F., Leaver, C.J. (2011) Sphingolipid long chain base phosphates can regulate apoptotic-like programmed cell death in plants. Biochem. Biophys. Res. Commun. **410**: 574–580.

Alexander, M.P. (1969) Differential stainig of aborted and non aborted pollen. Stain Technol. **44**:117-122.

Bi, F.C., Liu, Z., Wu, J.X., Liang, H., Xi, X.L., Fang, C., Sun, T.J., Yin, J., Dai, G.Y., Rong, C., Greenberg, J.T., Su, W.W., Yao, N. (2014) Loss of ceramide kinase in Arabidopsis impairs defenses and promotes ceramide accumulation and mitochondrial H_2O_2 bursts. Plant cell, **26**: 3449–67.

Bligh, E.G., Dyer, W.J. (1959) A rapid method of total lipid extraction and purification. Can. J. Biochem Physiol **37**: 911-917.

Breslow, D.K., Collins, S.R., Bodenmiller, B., Aebersold, R., Simons,

K., Shevchenko, A., Ejsing, C.S., Weissman, J.S. (2010) Orm family proteins mediate sphingolipid homeostasis. Nature, **463**:1048–1053.

Chen, M., Han, G., Dietrich, C.R., Dunn, T.M., Cahoon, E.B. (2006) The essential nature of sphingolipids in plants as revealed by the functional identification and characterization of the Arabidopsis LCB1 subunit of serine palmitoyltransferase. Plant Cell, **18**: 3576–3593.

Chen, M., Markham, J.E., Dietrich, C.R., Jaworski, J.G., Cahoon, E.B. (2008) Sphingolipid Long-Chain Base Hydroxylation Is Important for Growth and Regulation of Sphingolipid Content and Composition in Arabidopsis. Plant Cell, **20**:1862–1878.

Chen, M., Cahoon, E.B., Saucedo-García, M., Plasencia, J., Gavilanes-Ruíz, M. (2009) Plant Sphingolipids: Structure, Synthesis and Function. In H. Wada, N. Murata, eds, Lipids in Photosynthesis: Essential and Regulatory Functions. Springer Netherlands, Dordrecht, pp 77-115.

Chueasiri, C., Chunthong, K., Pitnjam, K., Chakhonkaen, S., Sangarwut, N., Sangsawang, K., Suksangpanomrung, M., Michaelson, L.V., Napier, J.A., Muangprom, A. (2014) Rice ORMDL controls sphingolipid homeostasis affecting fertility resulting from abnormal pollen development. PloS One 5;9(9):e106386.

Clarke BA, Majumder S, Zhu H, Lee YT, Kono M, Li C, Khanna C, Blain H, Schwartz R, Huso VL, Byrnes C, Tuymetova G, Dunn TM, Allende ML, Proia RL. (2019) The Ormdl genes regulate the sphingolipid synthesis pathway to ensure proper myelination and neurologic function in mice. eLife **8**:e51067.

Clough, S.J., Bent, A.F. (1998) Floral dip : a simplified method for Agrobacterium-mediated transformation of *Arabidopsis thaliana*. Plant J. **16**:735-43.

Coursol, S., Fan, L.M., Le Stunff, H., Spiegel, S., Gilroy, S., Assmann, S.M. (2003)

694 Sphingolipid signalling in Arabidopsis guard cells involves heterotrimeric G proteins.',
695 Nature, **423**:651-4.
696
697 **Dadsena, S., Bockelmann, S., Mina, J.G.M., Hassan, D.G., Korneev, S., Razzera,**
698 **G., Jahn, H., Niekamp, P., Müller, D., Schneider, M., Tafesse, F.G., Marrink,**
699 **S.J., Melo, M.N., Holthuis, J.C.M.** (2019) Ceramides bind VDAC2 to trigger
700 mitochondrial apoptosis. *Nat. Commun.* **10**:1832.
701
702 **Davis, D.L., Gable, K., Suemitsu, J., Dunn, T.M., Wattenberg, B.W.** (2019) The
703 ORMDL/Orm–serine palmitoyltransferase (SPT) complex is directly regulated by
704 ceramide: Reconstitution of SPT regulation in isolated membranes. J. Biol. Chem. **294**:
705 5146–5156.
706
707 **Davis, J.A., Pares, R.B., Bernstein, T., McDowell, S.C., Brown, E., Stubrich, J.,**
708 **Rosenberg, A., Cahoon, E.B., Cahoon, R.E., Poulsen, L.R., Palmgren, M.B., López-**
709 **Marqués, R.L., Harper, J.F.** (2020) The lipid flippases ALA4 and ALA5 play critical
710 roles in cell expansion and plant growth. Plant Physiol. pp.01332.02019.
711
712 **Dietrich, C.R., Han, G., Chen, M., Berg, R.H., Dunn, T.M., Cahoon, E.B.** (2008) Loss-
713 of-function mutations and inducible RNAi suppression of Arabidopsis LCB2 genes
714 reveal the critical role of sphingolipids in gametophytic and sporophytic cell viability.
715 Plant J. **54**:284-98.
716
717 **Gable, K., Slife, H., Bacikova, D., Monaghan, E., Dunn, T.M.** (2000) Tsc3p Is an 80-
718 amino acid protein associated with serine palmitoyltransferase and required for optimal
719 enzyme activity. J. Biol. Chem. **275**:7597–7603.
720
721 **Greenspan, P., Mayer, E.P., and Fowler, S.D.** (1985). Nile red - A selective
722 fluorescent stain for intracellular lipid droplets. J. Cell Biol. **100**: 965–973.
723
724 **Gupta, S.D., Gable, K., Alexaki, A., Chandris, P., Proia, R.L., Dunn, T.M., Harmon,**

J.M. (2015) Expression of the ORMDLS, modulators of serine palmitoyltransferase, is regulated by sphingolipids in mammalian cells. J. Biol. Chem. **290**: 90–98.

Han, G., Gupta, S.D., Gable, K., Bacikova, D., Sengupta, N., Somashekarappa, N., Proia, R.L., Harmon, J.M., Dunn, T.M. (2019) The ORMs interact with transmembrane domain 1 of Lcb1 and regulate serine palmitoyltransferase oligomerization, activity and localization. Biochim. Biophys. Acta Mol. Cell. Biol. Lipids **1864**:245–259.

Han, S., Lone, M.A., Schneiter, R., Chang, A. (2010) Orm1 and Orm2 are conserved endoplasmic reticulum membrane proteins regulating lipid homeostasis and protein quality control. Proc. Natl. Acad. Sci. U.S.A. **107**:5851-6.

Huby, E., Napier, J.A., Baillieul, F., Michaelson, L.V., Dhondt-Cordelier, S. (2020) Sphingolipids: towards an integrated view of metabolism during the plant stress response. New Phytol. **225**: 659-670.

Ischebeck, T. (2016) Lipids in pollen - They are different. Biochim. Biophys. Acta **1861**: 1315-1328.

Kimberlin, A.N., Majumder, S., Han, G., Chen, M., Cahoon, R.E., Stone, J.M., Dunn, T.M., Cahoon, E.B. (2013) Arabidopsis 56-Amino Acid Serine Palmitoyltransferase-Interacting Proteins Stimulate Sphingolipid Synthesis, Are Essential, and Affect Mycotoxin Sensitivity. Plant Cell. **25**: 4627–4639.

Kimberlin, A.N., Han, G., Luttgeharm, K.D., Chen, M., Cahoon, R.E., Stone J.M., Markham, J.E., Dunn, T.M., Cahoon, E.B. (2016) ORM expression alters sphingolipid homeostasis and differentially affects ceramide synthase activity. Plant physiol. **172**: 889–900.

Li, J., Yin, J., Rong, C., Li, K.E., Wu, J.X., Huang, L.Q., Zeng, H.Y., Sahu, S.K., Yao

N. (2016) Orosomucoid proteins interact with the small subunit of serine palmitoyltransferase and contribute to sphingolipid homeostasis and stress responses in Arabidopsis. Plant cell. **28**: 3038–3051.

Liang, H., Yao, N., Song, J.T., Luo, S., Lu, H., Greenberg, J.T. (2003) Ceramides modulate programmed cell death in plants. Genes Dev. **17**:2636-41.

Luttgeharm, K.D., Chen, M., Mehra, A., Cahoon, R.E., Markham, J.E., Cahoon, E.B. (2015a) Overexpression of Arabidopsis ceramide synthases differentially affects growth, sphingolipid metabolism, programmed cell death, and mycotoxin Resistance.', *Plant physiol.* **169**: 1108–17.

Luttgeharm, K.D., Kimberlin, A.N., Cahoon, R.E., Cerny, R.L., Napier, J.A., Markham, J.E., Cahoon, E.B. (2015b) Sphingolipid metabolism is strikingly different between pollen and leaf in Arabidopsis as revealed by compositional and gene expression profiling. Phytochemistry **115**: 121-129.

Mao, C., Xu, R., Bielawska, A., Obeid, L.M. (2000) Cloning of an alkaline ceramidase from Saccharomyces cerevisiae. An enzyme with reverse (CoA-independent) ceramide synthase activity. J. Biol. Chem. **275**:6876-84.

Markham, J.E., Li, J., Cahoon, E.B., Jaworski, J.G. (2006) Separation and identification of major plant sphingolipid classes from leaves. J. Biol. Chem. **281**:22684–94.

Markham, J.E., Jaworski, J.G. (2007) Rapid measurement of sphingolipids from *Arabidopsis thaliana* by reversed-phase high-performance liquid chromatography coupled to electrospray ionization tandem mass spectrometry. Rapid Commun Mass Spectrom **21**: 1304-1314

Markham, J.E., Molino, D., Gissot, L., Bellec, Y., Hématy, K., Marion, J., Belcram

K., Palauqui, J.C., Satiat-Jeunemaître, B., Faure, J.D. (2011) Sphingolipids containing very-long-chain fatty acids define a secretory pathway for specific polar plasma membrane protein targeting in Arabidopsis. Plant Cell**23**.:2362–2378.

Peer, M., Stegmann, M., Mueller, M.J., Waller, F. (2010) *Pseudomonas syringae* infection triggers *de novo* synthesis of phytosphingosine from sphinganine in *Arabidopsis thaliana.* FEBS Lett. **584**: 4053–4056.

Tantikanjana, T., Yong, J.W.H., Letham, D.S., Griffith, M., Hussain, M., Ljung, K., Sandberg, G., Sundaresan, V. (2001) Control of axillary bud initiation and shoot architecture in *Arabidopsis* through the SUPERSHOOT gene. Genes Dev. **15**: 1577–1588.

Teng, C., Dong, H., Shi, L., Deng, Y., Mu, J., Zhang, J., Yang X., and Zuo, J. (2008) Serine palmitoyltransferase, a key enzyme for *de novo* synthesis of sphingolipids, is essential for male gametophyte development in Arabidopsis. Plant Physiol. **146**: 1322–1332.

Ternes, P., Feussner, K., Werner, S., Lerche, J., Iven, T., Heilmann, I., Riezman, H., Feussner, I. (2011) Disruption of the ceramide synthase LOH1 causes spontaneous cell death in *Arabidopsis thaliana*. New Phytol. **192**:841–854.

Wang, Z.P., Xing, H.L., Dong, L., Zhang, H.Y., Han, C.Y., Wang, X.C., Chen, Q.J. (2015) Egg cell-specific promoter-controlled CRISPR/Cas9 efficiently generates homozygous mutants for multiple target genes in Arabidopsis in a single generation. Genome Biol. **16**:144.

Yang, F., Kimberlin, A.N., Elowsky, C.G., Liu, Y., Gonzalez-Solis, A. Cahoon, E.B., Alfano, J.R. (2019) A plant immune receptor degraded by selective autophagy. Mol. Plant. **12**:113–123.

Zheng, P., Wu, J.X., Sahu, S.K., Zeng, H.Y., Huang, L.Q., Liu, Z., Xiao, S., Yao, N. (2018) Loss of alkaline ceramidase inhibits autophagy in Arabidopsis and plays an important role during environmental stress response. Plant Cell Environ. **41**:837-849.

Zhu, L.H., Krens, F., Smith, M.A., Li, X., Qi, W., van Loo, E.N., Iven, T., Feussner, I., Nazarenus, T.J., Huai, D., Taylor, D.C., Zhou, X.R., Green, A.G., Shockey, J., Klasson, K.T., Mullen, R.T., Huang, B., Dyer, J.M., Cahoon, E.B. (2016) Dedicated Industrial Oilseed Crops as Metabolic Engineering Platforms for Sustainable Industrial Feedstock Production. Sci Rep **6**: 22181.

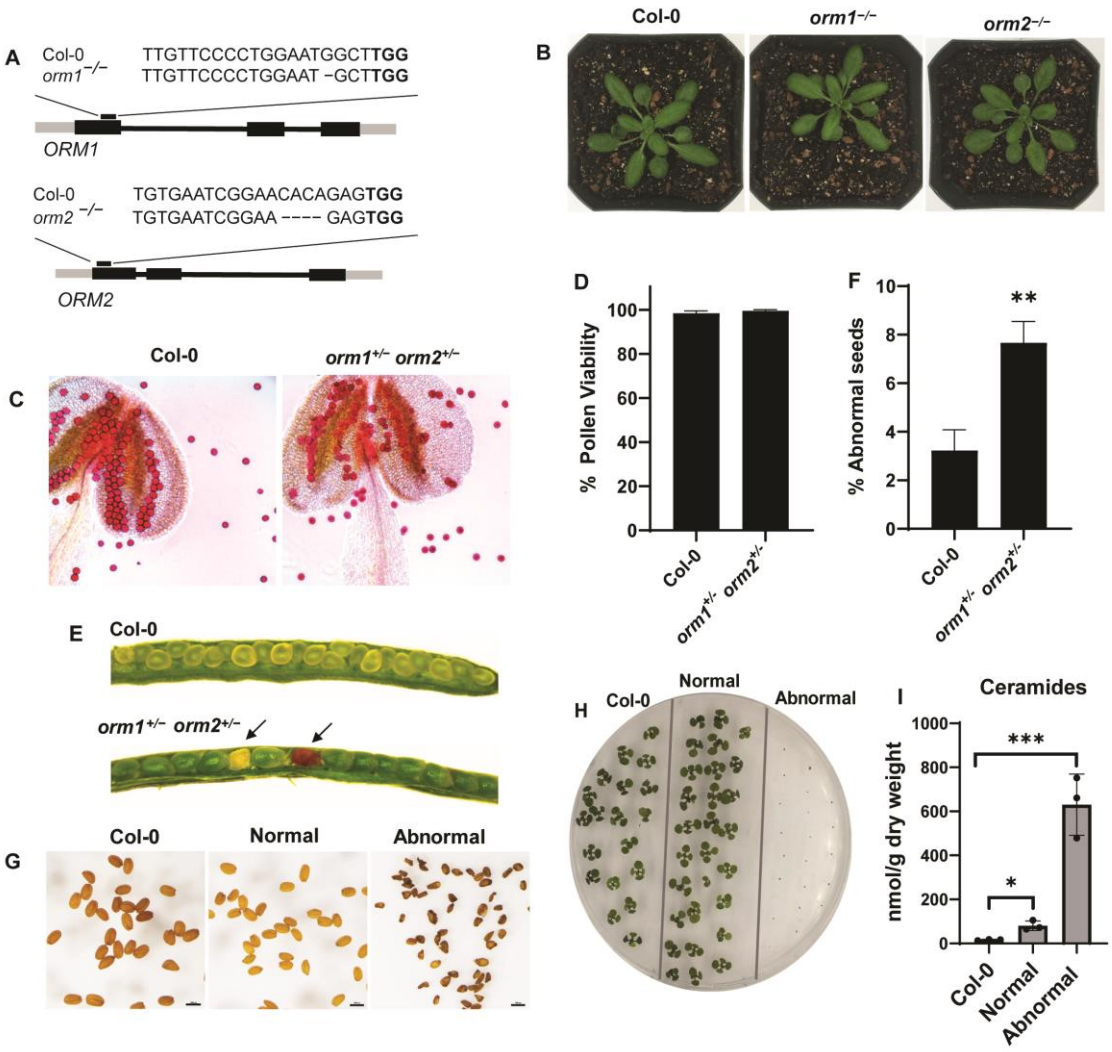

Figure 1. The ORM Double Knockout Mutant is Seed Lethal.

(A) Schematic representation of CRISPR/Cas9-induced mutations in *ORM* genes. Gene structures of *ORM1* and *ORM2*; black boxes represent exons. The CRISPR/Cas9 target site is indicated, as well as the nucleotide deletions for each gene in the single mutants.
(B) Representative images of 25-day-old wild-type Col-0, *orm1*$^{-/-}$ and *orm2*$^{-/-}$ plants.
(C) Representative images of pollen and anthers (treated with Allexander stain) collected from wild-type Col-0 and *orm1*$^{+/-}$ *orm2*$^{+/-}$ plants.
(D) Viability of pollen determined by counts of ~100 pollen grains from five randomly selected flowers from independent Col-0 and *orm1*$^{+/-}$ *orm2*$^{+/-}$ plants. Shown are the mean ± SD.
(E) Developing seeds in siliques from wild-type Col-0 and *orm1*$^{+/-}$ *orm2*$^{+/-}$ plants. Shriveled, brown (abnormal) seeds are indicated by arrows.
(F) Percentage of shriveled and brown (abnormal) seeds in siliques determined by counts of an average of 200 developing seeds from 10 randomly selected siliques of independent wild-type Col-0 and *orm1*$^{+/-}$ *orm2*$^{+/-}$ plants. Shown are the mean ± SD. Asterisks denote significant differences, as determined by two-tailed Student's *t* test with a significance of p ≤0.01.
(G) Seeds from wild-type Col-0; seeds from *orm1*$^{+/-}$ *orm2*$^{+/-}$ were separated and classified into normal and the darker, shriveled seeds as abnormal**.** Bars=1 mm.
(H) Phenotypes of 10-day-old seedlings from wild-type Col-0 seeds, normal and abnormal seeds from *orm1*$^{+/-}$ *orm2*$^{+/-}$. Abnormal seeds did not germinate.
(I) Ceramide content in seeds from wild-type Col-0, normal and abnormal seeds from *orm1*$^{+/-}$ *orm2*$^{+/-}$. Shown are the mean ± SD, n=3. Asterisks indicate significant differences based on one-way ANOVA followed by Tukey's multiple comparisons test, with a significance of (*) P≤0.05 and (***) P≤0.001.

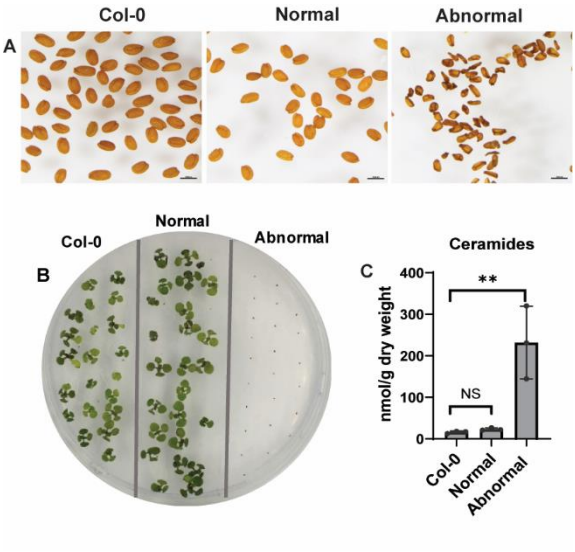

Figure 2. *Atlcb1*$^{+/-}$ Plants Expressing *LCB1ΔTMD1* Phenocopy the ORM Double Knockout Mutant.

(A) Seeds from wild-type Col-0; seeds from *Atlcb1*$^{+/-}$ plants expressing *LCB1ΔTMD1* were separated and classified into normal and abnormal darker and shriveled seeds. Bars=1 mm.
(B) Phenotypes of 10-day-old seedlings from wild-type Col-0 seeds, normal and abnormal seeds from *Atlcb1*$^{+/-}$ expressing *LCB1ΔTMD1*. Abnormal seeds did not germinate.
(C) Ceramide content in seeds from wild-type Col-0, normal and abnormal seeds from *LCB1ΔTMD1.* Shown are the mean ± SD, n=3. Asterisks indicate significant difference based on one-way ANOVA followed by Tukey's multiple comparisons test, (**) P≤0.01. NS, not significant.

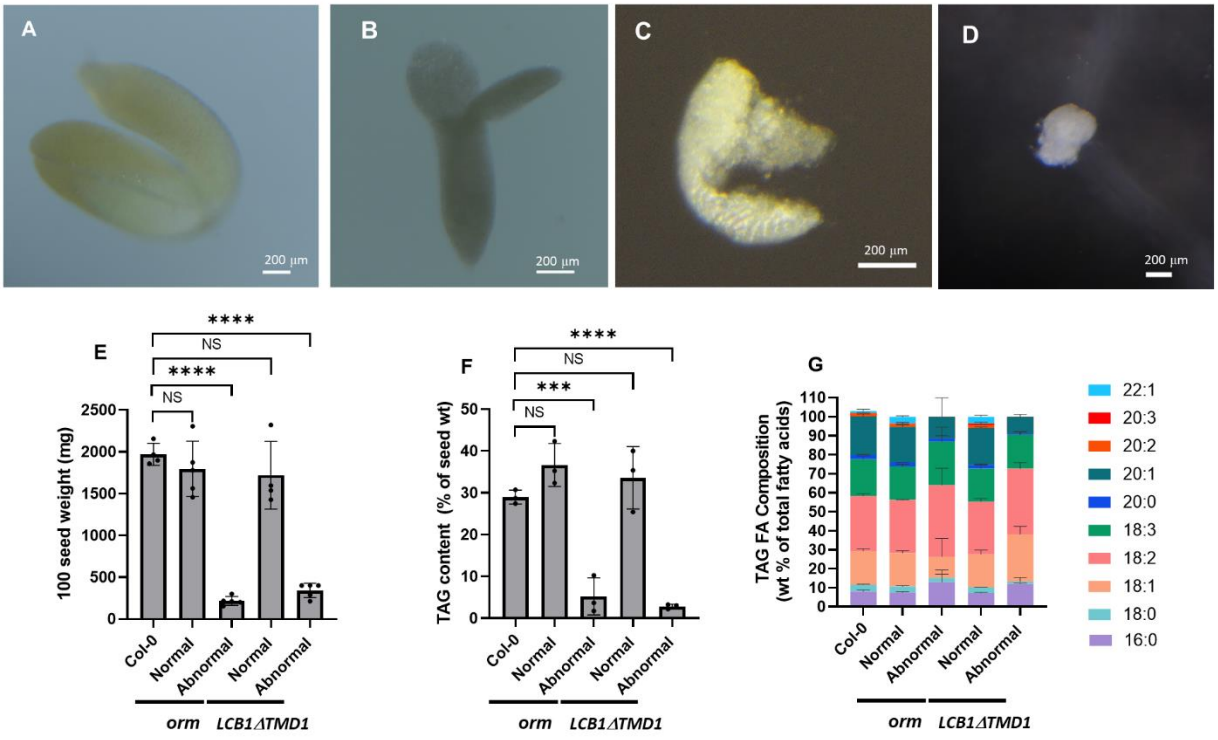

Figure 3. Abnormal Seeds from *ORM* and *LCB1ΔTMD1* Mutant Plants Have Altered Embryo Morphology and Reduced Triacylglycerol Concentrations.

Morphology of embryos from **(A)** wild-type seeds and **(B-D)** abnormal seeds from *orm1*$^{+/-}$ *orm2*$^{+/-}$ plants showing that the embryo is not fully developed. Embryos were dissected from mature seeds. Bars=200 µM.
(E) 100 seed weight. Values are the mean ± SD of seeds harvested from 4 independent plants. Asterisks indicate significant difference based on one-way ANOVA followed by Tukey's multiple comparisons test, with a significance of (****) P≤0.0001. NS, not significant.
(F) Triacylglycerol (TAG) content in seeds from wild-type Col-0 and normal and abnormal seeds from *orm1*$^{+/-}$ *orm2*$^{+/-}$ and *Atlcb1*$^{+/-}$ expressing *LCB1ΔTMD1.* Values are the mean ± SD of three independent lipid extractions. Asterisks indicate significant difference based on one-way ANOVA followed by Tukey's multiple comparisons test with a significance of (***) P≤0.001 and (****) P≤0.0001. NS, not significant.
(G) Composition of TAG as weight percent of fatty acid in seeds from wild-type Col-0 and normal and abnormal seeds from *orm1*$^{+/-}$ *orm2*$^{+/-}$ and *Atlcb1*$^{+/-}$ expressing *LCB1ΔTMD1*. Values are the mean ± SD of three independent samples.

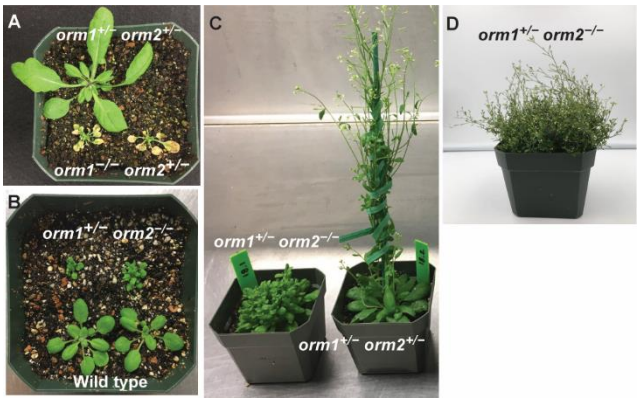

Figure 4. *orm1*$^{-/-}$ *orm2*$^{+/-}$ and *orm1*$^{+/-}$ *orm2*$^{-/-}$ Plants Have Distinct Growth Phenotypes.

(A) Representative image of 35-day-old *orm1*$^{+/-}$ *orm2*$^{+/-}$ and *orm1*$^{-/-}$ *orm2*$^{+/-}$ plants. The *orm1*$^{-/-}$ *orm2*$^{+/-}$ plants showed reduced size and yellow regions corresponding to cell death.
(B) Representative image of 18-day-old wild-type Col-0 and *orm1*$^{+/-}$ *orm2*$^{-/-}$ plants. Mutants showed reduced size, abnormal leaf shape, and a bushy phenotype.
(C) Representative image of 50-day-old *orm1*$^{+/-}$ *orm2*$^{-/-}$ and *orm1*$^{+/-}$ *orm2*$^{+/-}$ plants. The *orm1*$^{+/-}$ *orm2*$^{-/-}$ plants showed a bushy phonotype and delayed flowering.
(D) Representative image of 80-day-old *orm1*$^{+/-}$ *orm2*$^{-/-}$ plant.

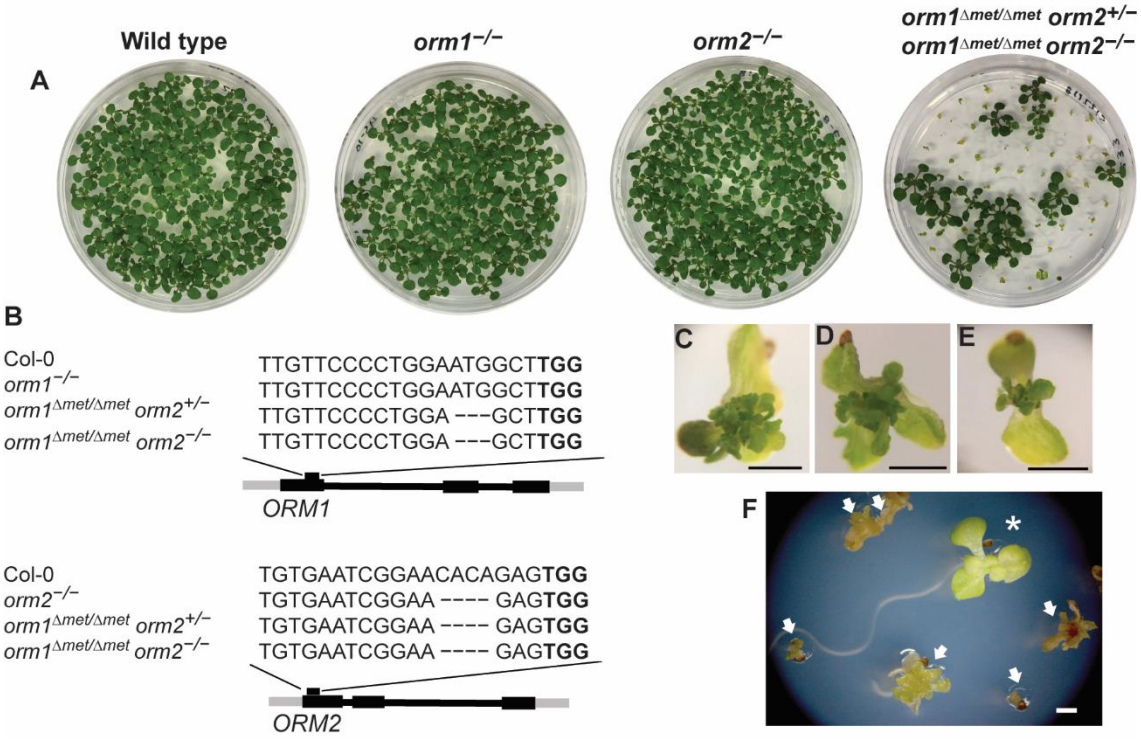

Figure 5. *orm1$^{\Delta met/\Delta met}$ orm2$^{-/-}$* Plants Exhibit Developmental Defects and Do Not Progress Beyond the Seedling Stage.

(A) Representative images of 12-day-old wild-type Col-0, *orm1$^{-/-}$*, *orm2$^{-/-}$*, *orm1$^{\Delta met/\Delta met}$ orm2$^{+/-}$* and *orm1$^{\Delta met/\Delta met}$ orm2$^{-/-}$* seedlings. Seedlings with the same phenotype as wild type correspond to *orm1$^{\Delta met/\Delta met}$ orm2$^{+/-}$*; small seedlings showing developmental defects correspond to *orm1$^{\Delta met/\Delta met}$ orm2$^{-/-}$*; enlarged images are shown in **(C-E)**. Bars=1 mm.
(B) CRISPR/Cas9-induced mutations in *ORM1* and *ORM2*. Structures of the ORM genes; black boxes represent exons. The position of the CRISPR target site is marked, as well as the nucleotide deletions in each mutant.
(F) Phenotypes of 18-day-old seedlings; arrows indicate *orm1$^{\Delta met/\Delta met}$ orm2$^{-/-}$* and asterisk indicates *orm1$^{\Delta met/\Delta met}$ orm2$^{+/-}$*. Bar= 1 mm.

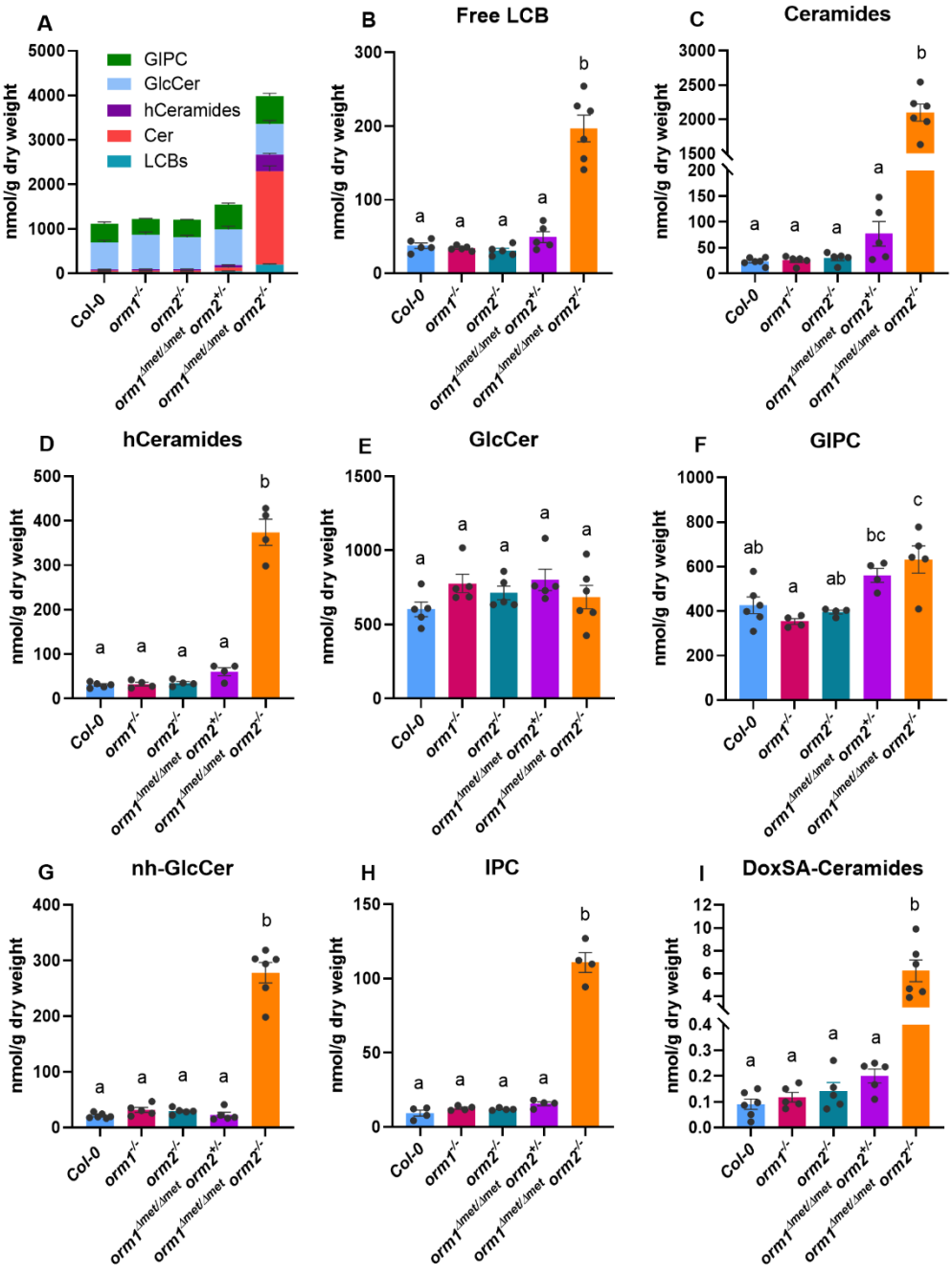

Figure 6. Selected Sphingolipid Classes Highly Accumulate in the *orm1*$^{\Delta met/\Delta met}$ *orm2*$^{-/-}$ Mutant.

(A) Total sphingolipid content in wild-type, *orm1*$^{-/-}$, *orm2*$^{-/-}$, *orm1*$^{\Delta met/\Delta met}$ *orm2*$^{+/-}$ and *orm1*$^{\Delta met/\Delta met}$ *orm2*$^{-/-}$. Content of the following sphingolipid classes in the mutants: **(B)** free LCBs, **(C)** ceramides with non hydroxylated fatty acids (Ceramides), **(D)** ceramides with hydroxylated fatty acids (hCeramides), **(E)** glucosylceramides (GlcCer), and **(F)** glycosylinositolphosphoceramides (GIPCs). Content of atypical sphingolipids **(G)** glucosylceramides with non-hydroxylated FA (nhGlcCer) and **(H)** inositol phosphorylceramides (IPCs). **(I)** Content of atypical deoxy-LCB m18:0 in ceramides. Normally, SPT condenses Serine with palmitoyl-CoA to form d18:0. However, the unusual condensation of Alanine gives rise to a deoxy-LCB, deoxy-sphinganine (DoxSA) m18:0. Measurements are the average of four to six replicates consisting of pooled 12 to 15-day-old seedlings grown on different plates. Bars represent standard error of the mean. Different letters indicate significant difference based on one-way ANOVA followed by Tukey's multiple comparisons test (P≤0.05).

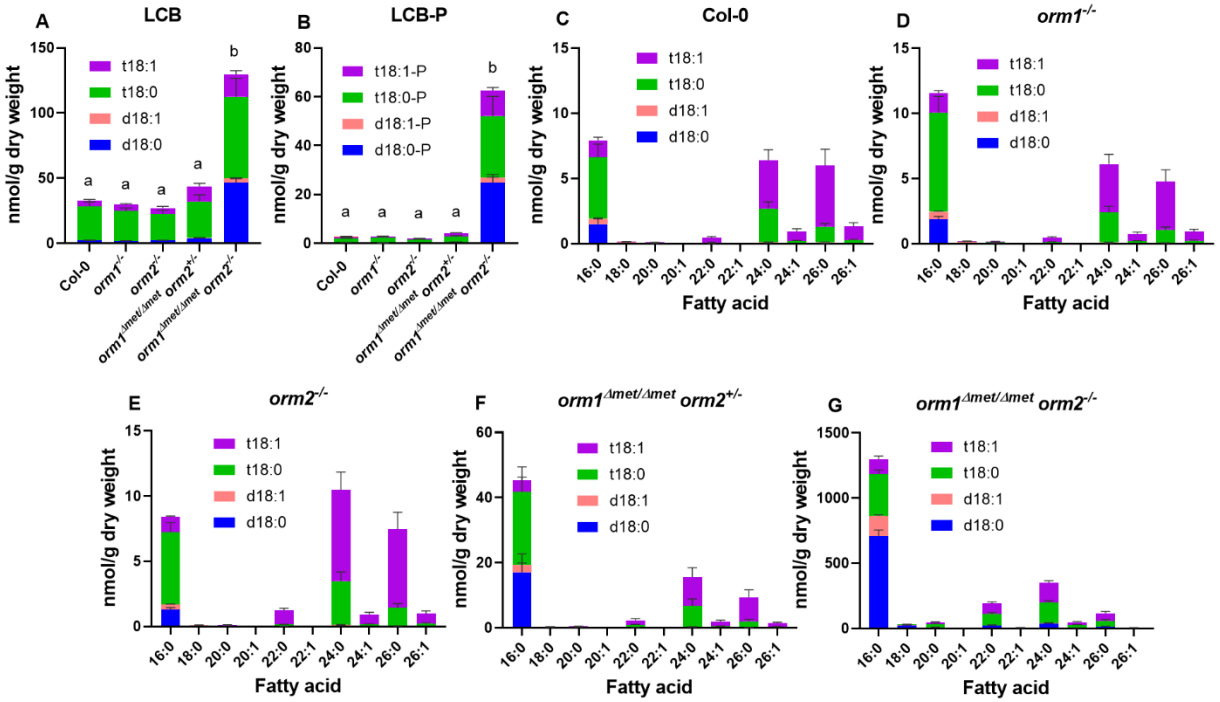

Figure 7. Free Long-Chain Base and Ceramide Compositions and Concentrations are Strongly Affected in the *orm1*$^{\Delta met/\Delta met}$ *orm2*$^{-/-}$ Mutant.

(A) Free long-chain base (LCB) composition (d18:0, d18:1, t18:0, t18:1) and **(B)** free LCB-phosphate (LCB-P) in wild-type, *orm1*$^{-/-}$, *orm2*$^{-/-}$, *orm1*$^{\Delta met/\Delta met}$ *orm2*$^{+/-}$ and *orm1*$^{\Delta met/\Delta met}$ *orm2*$^{-/-}$. Bars show averages of four to six replicates consisting of 12 to 15-day-old pooled seedlings grown on different plates. Error bars represent the standard error of the mean. Different letters indicate significant difference, for each LCB, based on one-way ANOVA followed by Tukey's multiple comparisons test (P≤0.05). Ceramide molecular species compositions representing the exact pairings of LCB and fatty acid for **(C)** wild type, **(D)** *orm1*$^{-/-}$, **(E)** *orm2*$^{-/-}$, **(F)** *orm1*$^{\Delta met/\Delta met}$ *orm2*$^{+/-}$ and **(G)** *orm1*$^{\Delta met/\Delta met}$ *orm2*$^{-/-}$ plants. Measurements for all panels are the average of four to six replicates consisting of 12 to 15-day-old pooled seedlings grown on different plates. Bars represent standard error of the mean.

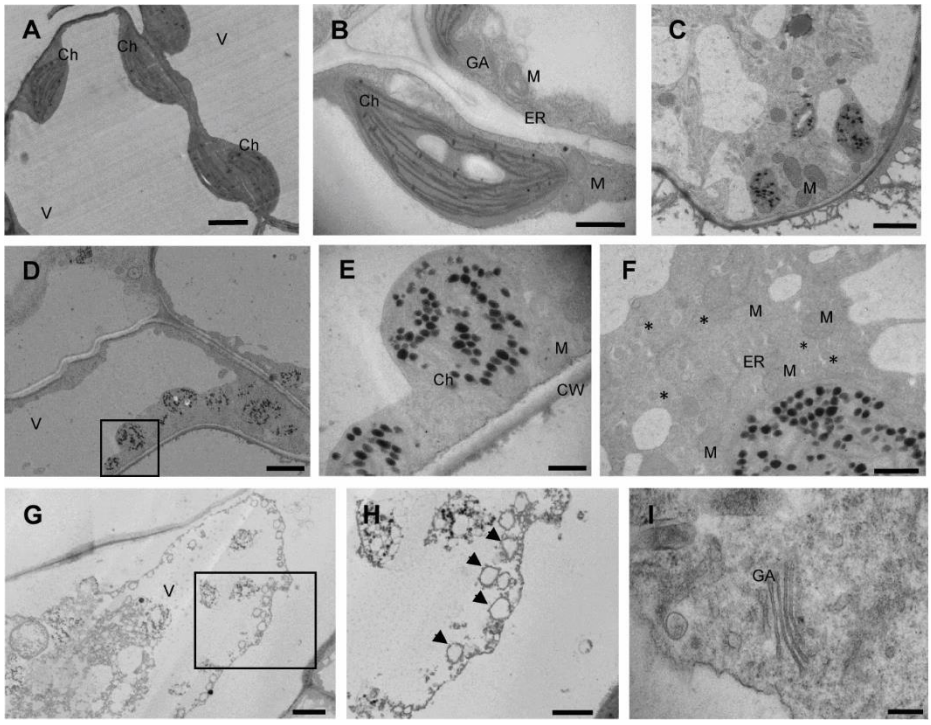

Figure 8. Subcellular Features are Strongly Altered in the *orm1*$^{\Delta met/\Delta met}$ *orm2*$^{-/-}$ Mutant.

Representative TEM images of **(A** and **B)** wild-type seedlings and **(C-I)** *orm1*$^{\Delta met/\Delta met}$ *orm2*$^{-/-}$. Longitudinal sections of leaves from ten-day-old seedlings were prepared for TEM analysis. Boxes represent sections enlarged in **(E)** and **(H)**. GA, Golgi apparatus; Ch, Chloroplast; CW, cell wall; ER, endoplasmic reticulum; M, mitochondrion; V, vacuole. Asterisks indicate vesicles and arrows autophagosomes. Bars= 200 nm in **(I)**, 800 nm in **(E)** and **(F)**, 1 μm in **(B)**, 2 μm in (**A)** and **(C)**, 4 μm in **(D)** and **(G)**.

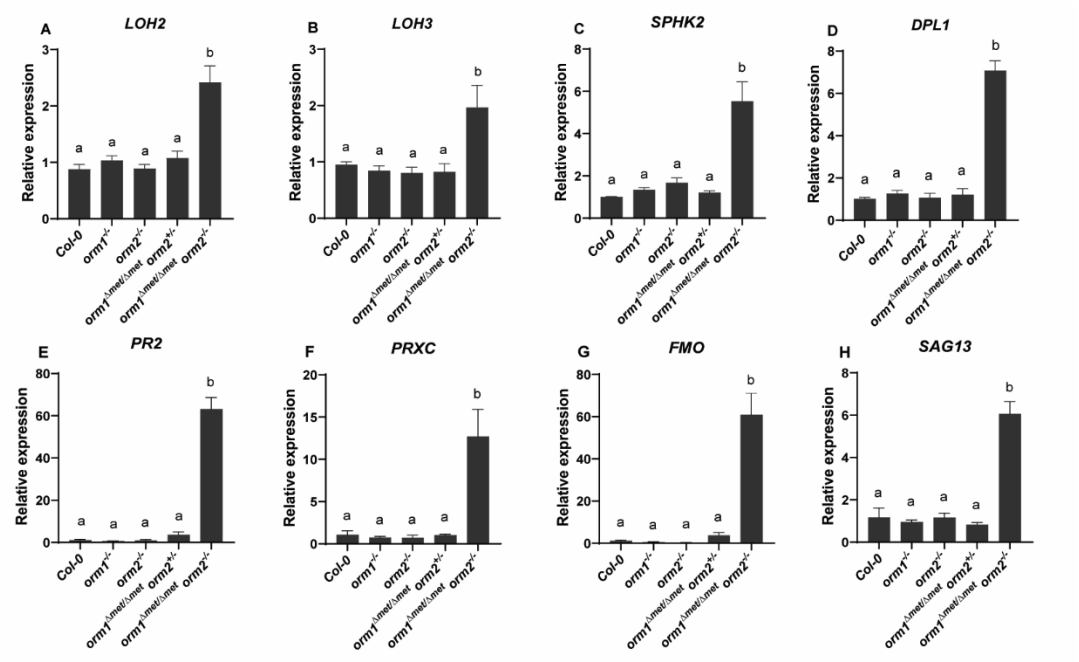

Figure 9. Expression of Genes Associated with Sphingolipid Homeostasis, Plant Defense Responses, and Senescence are Upregulated in the *orm1*$^{\Delta met/\Delta met}$ *orm2*$^{-/-}$ Mutant.

Wild-type, *orm1*$^{-/-}$, *orm2*$^{-/-}$ *orm1*$^{\Delta met/\Delta met}$ *orm2*$^{+/-}$ and *orm1*$^{\Delta met/\Delta met}$ *orm2*$^{-/-}$ seedlings (12-day-old plants) were used to examine gene expression by qPCR to monitor genes encoding enzymes in sphingolipid biosynthetic and catabolic pathways: **(A)** ceramide synthase gene *LOH2,* **(B)** ceramide synthase gene *LOH3*, **(C)** sphingosine kinase 2 gene *SPHK2* and **(D)** LCB phosphate lyase gene *DPL1;* and selected pathogenesis- and senescence-related genes: **(E)** β-1,3-glucanase gene *PR2*, **(F)** class III peroxidase gene *PRXC*, **(G)** flavin monooxygenase gene *FMO* and **(H)** senescence-related 13 gene *SAG13*. *PP2AA3* transcript levels were used as a control for the sphingolipid genes and *UBIQUITIN* for the pathogenesis and senescence-related genes. Specific primers used for this analysis are shown in Supplemental Table 1. Gene expression levels are normalized to those in wild-type seedlings. Values are the mean ± SD (n=6-12). Different letters indicate significant difference based on one-way ANOVA followed by Tukey's multiple comparisons test (P≤0.05).

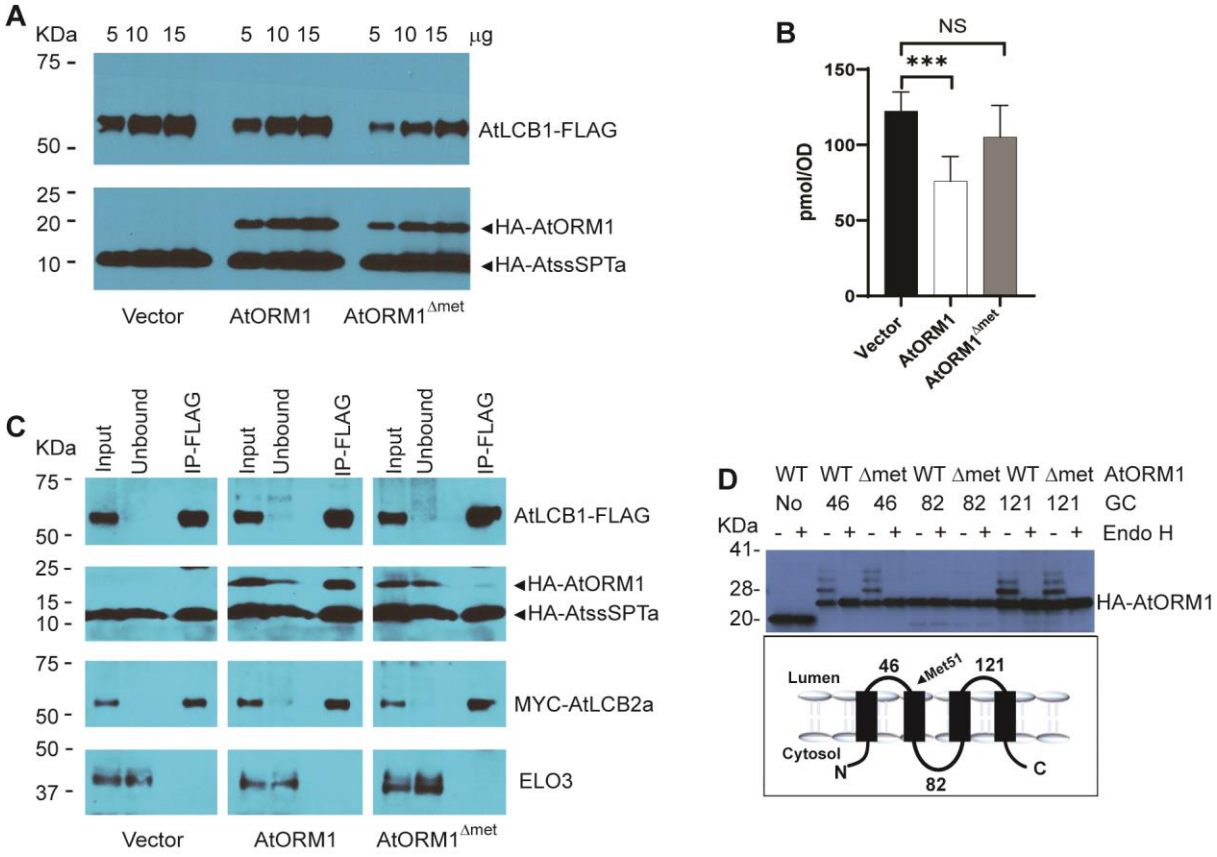

Figure 10. AtORM1$^{\Delta met}$ Fails to Regulate SPT Activity and Does Not Interact with LCB1.

(A) AtORM1$^{\Delta met}$ was stably expressed in *Saccharomyces cerevisiae* with the native SPT complex replaced by the Arabidopsis SPT complex (see Methods). AtLCB1-FLAG, MYC-AtLCB2a, HA-AtssSPTa without or with HA-AtORM1 or HA-AtORM1$^{\Delta met}$ were expressed in yeast strain *lcb1 tsc3.* 5, 10 and 15 µg of microsomal proteins were loaded and analyzed by SDS-PAGE (4-12%, Invitrogen) and detected with Anti-LCB1 (1:3000) and anti-HA antibodies (Covance).
(B) DoxSA levels were determined from cells expressing AtLCB1^{C144W} and AtLCB2a, HA-AtssSPTa along with vector, HA-AtORM1 wild-type, or HA-AtORM1$^{\Delta met}$. Shown are the mean ± SD of doxSA levels from six independent colonies for each strain. Asterisks denote significant differences, as determined by two-tailed Student's *t* test with a significance of $p \leq 0.001$; NS, not significant, n=6.
(C) Co-immunoprecipitation of FLAG-tagged AtLCB1 in yeast expressing AtLCB1-FLAG, MYC-AtLCB2a, HA-AtssSPTa, and either HA-AtORM1 or HA-AtORM1$^{\Delta met}$. Solubilized yeast microsomes were incubated with anti-FLAG beads and protein was eluted with FLAG peptide. Solubilized microsomes (Input), unbound and bound (IP-FLAG) were analyzed by immunoblotting. ELO3, an integral ER membrane protein, was used as a negative control.
(D) Topology mapping of AtORM1$^{\Delta met51}$. Glycosylated cassettes (GC) were inserted after the indicated amino acids, and the GC-tagged proteins were expressed in yeast. Increased mobility following treatment of microsomes with endoglycosidase H (EndoH) revealed that the GCs at residues 46 and 121 are glycosylated and therefore reside in the lumen of the endoplasmic reticulum. However, the GC at residue 82 is not glycosylated, indicating that residue 82 is located in the cytosol. AtORM1$^{\Delta met51}$ retains the topology of wild-type ORM1.

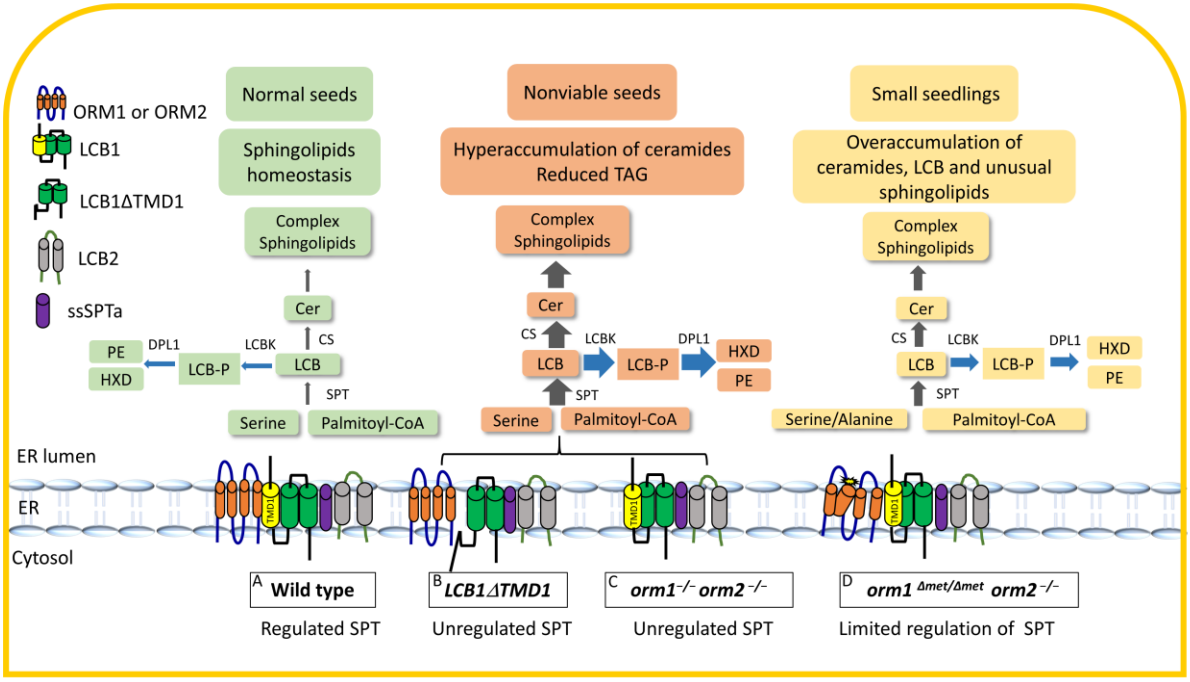

Figure 11. Model of ORM-Mediated Sphingolipid Biosynthesis in Wild-type Plants and *ORM* and *LCB1* Mutants.

ORM proteins and LCB1 are integral ER-membrane proteins with multiple transmembrane domains (TMDs). The ORM proteins contain four TMDs, with both termini located in the cytosol, while LCB1 has three TMDs, with its N-terminus located in the ER-Lumen and C-terminus located in the cytosol. LCB1, along with LCB2 and ssSPTa, comprise serine palmitoyltransferase (SPT), which catalyzes the first step in sphingolipid biosynthesis. TMD1 of LCB1 is required for ORM binding to SPT (A). Expression of LCB1 without its first transmembrane domain (B) or the complete knockout of *ORM1* and *2* (C) results in the loss of SPT regulation. This is characterized by strongly enhanced accumulation of ceramides and selected complex sphingolipids and the loss of seed viability marked by a strong reduction in TAG content. The lack of MET51 before the second transmembrane domain (TMD2) of ORM1 it thought to causes a conformational change that dramatically decreases its interaction with LCB1 for SPT regulation (D). CS, ceramide synthase; LCB, long chain bases; LCB-P, long chain bases-phosphate; CER, ceramide; LCBK, long chain base kinase: DPL1, LCB phosphate lyase; PE, phosphoethanolamine; HXD, hexadecanal. Black arrows indicate *de novo* sphingolipid biosynthesis and blue arrows indicate catabolic reactions.

Unregulated Sphingolipid Biosynthesis in Gene-Edited Arabidopsis ORM Mutants Results in Nonviable Seeds with Strongly Reduced Oil Content

Ariadna Gonzalez Solis, Gongshe Han, Lu Gan, Yunfeng Liu, Jonathan E. Markham, Rebecca E. Cahoon, Teresa M. Dunn and Edgar B. Cahoon

Plant Cell; originally published online June 11, 2020;
DOI 10.1105/tpc.20.00015